Rhinovirus reduces the severity of subsequent respiratory viral infections by interferon-dependent and -independent mechanisms

James T. Van Leuven[1,2†], Andres J. Gonzalez[1,2†], Emmanuel C. Ijezie[1,2†], Alexander Q. Wixom[3#], John L. Clary[1,2], Maricris N. Naranjo[2,4], Benjamin J. Ridenhour[1,5], Craig R. Miller[1,2], and Tanya A. Miura[1,2*]

[1] Institute for Modeling Collaboration and Innovation, University of Idaho, Moscow, ID, USA
[2] Department of Biological Sciences, University of Idaho, Moscow, ID, USA
[3] Department of Plant Sciences, University of Idaho, Moscow, ID, USA
[4] Division of Natural Sciences, University of Guam, Mangilao, GU, USA
[5]Department of Mathematics, University of Idaho, Moscow, ID, USA

[*]Corresponding author E-mail: tmiura@uidaho.edu
†These authors contributed equally to this work.
[#]Current Address: Department of Gastroenterology and Hepatology, Mayo Clinic, Rochester, MN, USA

Abstract

Coinfection by unrelated viruses in the respiratory tract is common and can result in changes in disease severity compared to infection by individual virus strains. We have previously shown that inoculation of mice with rhinovirus (RV) two days prior to inoculation with a lethal dose of influenza A virus (PR8), provides complete protection against mortality and reduces morbidity. In this study, we extended that finding to a second lethal respiratory virus, pneumonia virus of mice (PVM) and analyzed potential mechanisms whereby RV reduces lethal viral pneumonia caused by PR8 and PVM. RV prevented mortality and weight loss associated with PVM infection, suggesting that RV-mediated protection is more effective against PVM than PR8. Major changes in host gene expression upon PVM infection were delayed compared to PR8, which likely provides a larger time frame for RV-induced gene expression to alter the course of disease. Overall, RV induced earlier recruitment of inflammatory cells, while these populations were reduced at later times in RV-inoculated mice. Findings common to both virus pairs included upregulated expression of mucin-associated genes and dampening of inflammation-related genes

in mice that were inoculated with RV prior to lethal virus infection. However, type I IFN signaling was required for RV-mediated protection against PR8, but not PVM. IFN signaling had minor effects on PR8 replication and contributed to controlling neutrophilic inflammation and subsequent hemorrhagic lung pathology in RV/PR8 infected mice. These findings, combined with differences in virus replication levels and disease severity, suggest that the suppression of inflammation in RV/PVM infected mice may be due to early, IFN-independent suppression of viral replication, while in RV/PR8 infected mice may be due to IFN-dependent modulation of immune responses. Thus, a mild upper respiratory viral infection can reduce the severity of a subsequent severe viral infection in the lungs through virus-dependent mechanisms.

Author Summary

Respiratory viruses from diverse families co-circulate in human populations and are frequently detected within the same host. Though clinical studies suggest that infection by more than one unrelated respiratory virus may alter disease severity, animal models in which we can control the doses, timing, and strains of coinfecting viruses are critical to understand how coinfection affects disease severity. In this study, we compared gene expression and immune cell recruitment between two pairs of viruses (RV/PR8 and RV/PVM) inoculated sequentially in mice that both result in reduced severity compared to lethal infection by PR8 or PVM alone. Reduced disease severity was associated with suppression of inflammatory responses in the lungs. However, differences in disease kinetics and host and viral gene expression suggest that protection by coinfection with RV may be due to distinct molecular mechanisms. Indeed, we found that antiviral cytokine signaling was required for RV-mediated protection against lethal infection by PR8, but not PVM.

56

57 ## Introduction

58 The detection of more than one virus in respiratory samples is quite common, especially
59 among pediatric patients (1-4). There are differences in the outcomes of coinfection - whether it
60 results in increased, decreased, or no effect on disease severity - that likely reflect different virus
61 parings, patient populations, and study criteria. For example, coinfection with influenza B virus
62 was found to increase the severity of seasonal influenza A virus, while other virus pairings did not
63 reach statistical significance (2). Another study found increased rates of hospitalization, but not
64 other measures of clinical severity, associated with viral coinfections (1). In contrast, Martin et al.
65 found that patients with one virus detected had increased risk of severe disease than those with
66 multiple viruses detected, and some virus pairings were associated with lower viral loads in
67 coinfected patients (5). Coinfection by non-SARS-CoV-2 viruses has been detected in COVID-19
68 patients, but the impact on disease severity is not well-understood (6-8). Recently, RV has been
69 shown to inhibit replication of SARS-CoV-2 in cultured human airway epithelial cells (9). Despite
70 differences among studies, it is clear that coinfecting viruses have the potential to alter
71 pathogenesis and disease outcomes. While clinical studies illuminate this potential, model systems
72 in which the virus pairs, doses, and timing of coinfection can be controlled are critical to
73 understand how coinfection alters pathogenesis in the respiratory tract. Therefore, we developed a
74 mouse model using pairwise combinations of respiratory viruses from different families for this
75 purpose (10).

76 We previously found that inoculation of mice with a mild respiratory virus (rhinovirus
77 strain 1B [RV] or mouse hepatitis virus strain 1 [MHV-1]) attenuates the severity of a subsequent
78 infection by influenza A virus (strain PR8) (10). Although pre-infection does not prevent PR8

79 replication, it leads to faster viral clearance and resolution of pulmonary inflammation. Protection
80 from severe disease by viral coinfection has also been demonstrated by other groups. Similar to
81 our study, Hua et al. found that a nasal-restricted infection by MHV-1 protects mice from lethal
82 infection by PR8 and mouse-adapted severe acute respiratory syndrome coronavirus (SARS-CoV)
83 (11). Furthermore, they found that protection is associated with enhanced macrophage recruitment
84 to the lungs and up-regulation of SARS-CoV-specific CD4+ and CD8+ T cell responses (11).
85 Inhibition or delay of viral shedding also occurs in ferrets during sequential inoculations with
86 antigenically similar or dissimilar strains of influenza A and B viruses (12). A 2009 pandemic
87 influenza A (A(H1N1)pdm09) virus prevents subsequent infection of ferrets by human respiratory
88 syncytial virus (RSV) when the viruses are given within a short time frame (13). In contrast, RSV
89 does not prevent replication of A(H1N1)pdm09 in ferrets, but reduces morbidity as determined by
90 weight loss (13). Inhibition of RSV by prior inoculation with influenza A virus has also been
91 demonstrated in mice (14).

92 In this study, we aimed to evaluate whether RV-mediated disease attenuation was specific
93 to PR8, or generalizable to other respiratory viral infections. We found that RV reduced the
94 severity of an additional lethal respiratory virus, pneumonia virus of mice (PVM). PVM is a
95 relative of human RSV in the family *Pneumoviridae*, genus *Orthopneumovirus*. Infection of mice
96 with PVM results in severe disease that shares clinical features of the most severe infections by
97 RSV, including infection of the bronchiolar epithelium, granulocytic inflammation, and
98 pulmonary edema (15-17). Lethality upon infection of mice with PR8 or PVM is mediated largely
99 by dysregulated inflammatory responses, rather than overt damage due to viral replication (18-21).
100 Interestingly, there are differences in the types of immune responses that mediate protection
101 against these two viruses. Type I and III interferon (IFN) signaling and alveolar macrophages are

102 protective in PR8-, but not PVM-, infected mice (18, 20, 22-25). Conversely, plasmacytoid
103 dendritic cells are required for protection in PVM-, but not PR8-, infected mice (26, 27).
104 Interleukin-6 (IL-6) limits the severity of influenza A virus infection in mice, while it exacerbates
105 disease in PVM-infected mice (28-30). Multiple mechanisms reduce the severity of both PR8 and
106 PVM infections, including mucin production and inhibition of inflammatory responses (31-37).
107 Based on these complex differences in immunity to infection with PR8 and PVM, we used a global
108 gene expression approach combined with flow cytometry to evaluate potential mechanisms
109 whereby pre-inoculation with RV reduces the severity of PR8 and PVM.
110

111 ## Results

112 **Inoculation of mice with RV reduces the severity of PVM infection**

113 We previously showed that inoculation of mice with RV completely prevented mortality
114 and reduced morbidity of a lethal infection by influenza A virus, strain PR8 (10). Protection against
115 lethal PR8 infection was most effective when RV was given two days before PR8, but significant
116 disease attenuation was also seen when mice were inoculated with RV and PR8 concurrently. To
117 determine if RV would attenuate disease by a second lethal respiratory viral pathogen, we
118 inoculated mice with media (mock) or RV two days before, simultaneously with, or two days after
119 inoculation with PVM. Mice were monitored daily for mortality, weight loss, and clinical signs of
120 disease for 14 days after PVM inoculation.

121 Infection with PVM alone (mock/PVM) was 100% lethal with all mice succumbing to
122 infection or reaching humane endpoints by day 8 (Fig 1A). PVM-infected mice had rapid weight
123 loss (Fig 1B) and exhibited clinical signs of disease, including ruffled fur, hunched posture, labored
124 breathing, and lethargy. Mice that were inoculated with RV two days before (RV/PVM) or

125 simultaneously with (RV+PVM) PVM were completely protected from mortality (Fig 1A), weight
126 loss (Fig 1B), and clinical signs of disease. However, mice that received RV two days after PVM
127 (PVM/RV) had equivalent disease severity as mock/PVM-infected mice. Although inoculation
128 with RV reduced the severity of both PR8 (10) and PVM (Fig 1), protection was more effective
129 against PVM. Importantly, complete protection against morbidity in addition to mortality was seen
130 when RV was given two days before or concurrent with PVM (Fig 1). In contrast, RV prevented
131 mortality, but not morbidity, when given two days before PR8 and inoculation of RV and PR8
132 concurrently was less effective at reducing disease severity (10).
133

134 **Infection by PR8 and PVM induce different gene expression signatures in mouse lungs over**
135 **time**
136
137 To determine potential mechanisms of protection mediated by RV against PR8 and PVM,
138 we undertook a comprehensive transcriptome analysis of mouse lungs (Fig 2). Mice were
139 inoculated with RV two days before PR8 or PVM and RNA isolated from the right lobes was
140 analyzed on days 0, 2, 4, and 6 after PR8 or PVM inoculation. Single virus-infected mice were
141 mock-inoculated two days before PR8 or PVM. Weight loss was monitored daily to test for
142 consistency with our previous coinfection studies. RV-mediated protection against PR8 was not
143 evident by 6 days post-infection (S1 Fig) though both mock/PR8 and RV/PR8 groups experienced
144 weight loss at a rate similar to our previous study (10). In contrast, complete protection against
145 weight loss was evident in RV/PVM treated mice (S1 Fig).
146 Lung mRNA from 3 mice per infection group and time point was collected and sequenced
147 on the Illumina platform. Of the 14.6 to 55.3 (36.4 mean) million reads obtained for each sample,
148 83-91.2% were uniquely mapped to the mm10 mouse genome (GCA_000001635.2). The
149 expression of 24,243 and 24,421 genes were measured using Cufflinks and HTSeq, respectively.

150 We conservatively included differentially expressed genes (DEGs) by requiring that they be
151 identified by Cuffdiff, EdgeR, and Deseq2 as having a $\log_2$ fold change value of at least 0.5 and
152 *p*-value less than 0.05.

153 A principal component analysis (PCA) was done with the 500 most highly variable genes
154 to visualize variation across infection groups, time points, and replicates. For the most part,
155 replicate samples clustered together (Fig 3A). Most variation in host gene expression was
156 explained by the time elapsed since viral infection (Fig 3A). However, differences between viruses
157 were also apparent. Infection by PVM caused fewer gene expression changes at early time points
158 than PR8-infected mice, as seen by mock/PVM and RV/PVM day 2 samples clustering closely
159 with mock and RV day 0 samples, respectively (Fig 3A, blue and purple points). By day 4, the
160 PVM-infected mice had very different gene expression profiles than mock-inoculated mice on day
161 0. This delayed response to PVM infection is observed in other studies (18, 38). In contrast, PR8
162 infection dramatically altered gene expression in mice by day 2 (Fig 3A, light green points). Early
163 changes in host gene expression induced by PR8, but not PVM, corresponded with earlier detection
164 of PR8-specific transcripts (Fig 4). Moreover, the RV/PVM and mock/PVM samples were very
165 different from each other by day 4 (Fig 3A, brown points). RV/PR8 and mock/PR8 groups had
166 similar gene expression signatures until day 6 (Fig 3A, orange points). This corresponds with the
167 similar disease kinetics in the mock/PR8 and RV/PR8 groups early during infection (10) (S1 Fig).

168 We next calculated differential gene expression levels in samples from RV-inoculated mice
169 compared to mock-inoculated mice on day 0 (Fig 3B). Similar to the PCA, gene expression was
170 significantly changed 2 days post-infection with RV and the response was markedly skewed
171 towards up-regulation. DEGs identified in all infection groups vs. mock were compared between
172 single virus-infected and RV-treated mice at each time point (Fig 3C). Gene expression changed

173 over time, as samples taken 2 days post-infection were most similar to mock-inoculated controls
174 and samples taken 6 days post-infection were most different (Fig 3C, 3D). The transition of point
175 clustering in Fig 3C from around the origin at day 2 to spread along the 1:1 line on day 6 illustrates
176 this delayed gene expression response to viral infection. Genes that were differentially expressed
177 between single virus-infected and RV-treated mice also displayed time-dependent clustering shifts
178 in both the PVM and PR8 experiments (Fig 3C). At 2 days post-infection, the expression values
179 of DEGs indicated that the samples from RV/PR8 and RV/PVM groups were more different from
180 mock than the samples from single virus-infected mice (points are spread along the y-axis). At 6
181 days post-infection, DEGs differed more between mock-inoculated and single virus-infected mice
182 than between mock and RV-treated mice (points spread along x-axis). This dampening of DEGs
183 in RV/PR8 and RV/PVM groups suggests that infection by a lethal virus is ablated not only in
184 virulence, but also in host gene expression response.

185 A summary of the numbers of DEGs across comparisons of all virus-infected to mock-
186 inoculated mice and between single virus-infected vs. RV/PR8 or RV/PVM treated mice is shown
187 in Fig 3D and lists of these DEGs are included in Supplemental Table 1. Again, the numbers of
188 DEGs reflect the delayed response to PVM infection, dampened gene expression in RV/PR8 and
189 RV/PVM groups of mice, and relative similarity in gene expression in mock/PR8 and RV/PR8
190 infected mice early in infection.

191

192 **Viral gene expression**

193 Sequencing reads that did not map to the mouse genome were aligned with viral genomes.
194 An insignificant number of reads mapped to the RV genome. This was expected because the
195 abundance of positive-sense RV RNA and viral titers peak 24 hours after inoculation of BALB/c

196 mice (39). The earliest time we analyzed was 48 hours (day 0) after inoculation, at which point
197 RV RNA would likely represent a very low proportion of the total RNA. We confirmed this by
198 quantifying infectious RV in homogenized lung tissue and broncho-alveolar lavage fluid (BALF)
199 24 h and 48 h after RV inoculation, days -1 and 0, respectively. In agreement with published studies
200 and our RNA-seq results, low levels of RV were detected on day -1, but not day 0 (S10 Fig). Thus,
201 we cannot conclude that RV is replicating in mouse lungs despite having a significant impact on
202 host gene expression.

203 Many reads mapped to PR8 and PVM genomes from the mice infected with these viruses
204 (Fig 4). Regression analyses were performed to identify significant changes over time (S3 Table).
205 Pre-treatment with RV did not prevent PR8-specific gene expression, but reads mapped to PR8
206 were lower in RV/PR8 mice at all time points (Fig 4A). When this analysis was expanded to
207 additional animals assayed by RT-qPCR for the HA gene, RV/PR8 infected mice only had
208 significantly lower viral gene expression compared to mock/PR8 infected mice on day 6 (Fig 4B),
209 which was also the time point that was most dramatically different in RNA-seq reads. Similarly,
210 we previously showed that infectious PR8 titers in the lungs were equivalent in mock/PR8 and
211 RV/PR8 infected mice on days 2 and 4 after PR8 inoculation (10). However, incoulation with RV
212 led to earlier clearance of PR8 (by day 7), corresponding with the dramatically lower PR8 mRNAs
213 seen on day 6 in the present study. These findings confirm that infection with RV does not prevent
214 subsequent infection by PR8, rather it reduces viral gene expression, specifically late during
215 infection. Our sequencing protocol only captured polyadenylated RNAs, thus the PR8 reads
216 represent viral mRNAs and not complementary (cRNA) or genomic (vRNA) viral RNAs, while
217 RT-qPCR was performed on total RNA. Based on individual gene mapping, the PR8 reads

218 predominantly mapped to the nucleoprotein (NP) and hemagglutinin (HA) mRNAs (S2 Fig),
219 which are known to be expressed at high levels during infection (40-42).

220 PVM gene expression was highest on day 4, but was robustly suppressed in RV-inoculated
221 mice (Fig 4). This trend was confirmed by RT-qPCR quantification of the PVM SH gene (Fig 4B)
222 and quantification of infectious virus (see Fig 8E), below. This suggests that RV may limit PVM
223 infection early, which corresponds with the more effective prevention of weight loss in RV/PVM
224 (Fig 1) compared to RV/PR8 (10) infected mice (S1 Fig). All viral genes were detected in mice
225 infected by PVM alone (mock/PVM) on day 4, with the genes that express the attachment (G),
226 nucleoprotein (N), non-structural 2 (NS2), fusion (F), phosphoprotein (P), and matrix (M) proteins
227 at the highest levels (S2 Fig). This does not strictly follow the gradient of mRNA levels
228 corresponding with gene order that is expected from pneumoviruses (43), which likely reflects
229 post-transcriptional differences in mRNA stability and the heterogeneous nature of collecting cells
230 at different stages of the virus replication cycle.

231

232 **RV induces innate immune response prior to secondary viral infection**

233 We compared gene expression in lung tissue of mock-inoculated mice to mice inoculated
234 with RV for 2 days (RV, day 0). Of the 24,421 genes compared, we identified 330 DEGs, of which
235 only three were down-regulated (Fig 3B, 3D, and S1 Table). To get a functional picture of the RV-
236 treated lung on day 0, we identified enriched GO terms and KEGG pathways in the 330 DEGs.
237 The most highly enriched terms on this list suggest that changes in the regulation of cell cycle or
238 cell division were occurring in RV- compared to mock-inoculated mice; nearly all of the top 50
239 most enriched terms involved chromosome remodeling and mitosis (S2 Table), suggesting RV-
240 induced increase in cellular proliferation. This list of enriched terms was quite different than the

241 processes that were differentially regulated in PR8- or PVM-infected mice. Up-regulation of cell
242 division-associated genes could be occurring in epithelial cells in conjunction with repair, immune
243 cells recruited to the lungs, or both. In addition to cell division, multiple immune response-related
244 GO terms related to type I IFN signaling, chemokine signaling, and immune cell chemotaxis were
245 enriched in RV-treated mice (S2 Table). RV induced up-regulation of several chemokine genes,
246 including those that recruit monocytes, neutrophils, NK cells, T cells, B cells, and eosinophils
247 (Ccl-2, 3, 6, 7, 8, 12, 17, 22, Cxcl-1, 3, 5, 9, 10, 13).
248
249 **Host gene expression changes in RV/PR8 and RV/PVM infected mice**
250 We next identified DEGs specific to mice exposed to two viruses (RV/PR8 or RV/PVM)
251 vs. mock-inoculated mice that were not differentially expressed in single virus-infected
252 (mock/PR8 or mock/PVM) vs. mock-inoculated mice at the same time points. The expression data
253 for these three gene sets (unique to RV/PR8, unique to RV/PVM, shared by RV/PR8 and
254 RV/PVM) are provided in supplemental figures (Fig S3-S5). Genes with shared up-regulation in
255 RV-inoculated animals, regardless of time point and second virus, included those in the mucin
256 biosynthesis pathway, MHC class II genes, and immunomodulatory genes. Genes with increased
257 up-regulation in mice infected with RV/PVM compared to mock/PVM early (days 2 and 4)
258 included Mgl2, Ccl6, Agr2, H2-M2, and Muc5b. Genes that had higher up-regulation in the single
259 virus infections were predominantly increased late (days 4 and/or 6) and included genes associated
260 with inflammation (Angptl4) or pulmonary fibrosis (Fosl2, Pappa, Sphk1). These genes were
261 common to both PR8 and PVM infections and likely result from excessive inflammation and tissue
262 damage within the infected lungs. Additional genes associated with inflammation and fibrosis
263 (Nfkbia and Mmp9) or stress responses (Hspb8, Nupr1) were reduced in RV/PVM- compared to

264 mock/PVM-infected mice. Finally, a set of genes were up-regulated in both mock/PVM- and
265 RV/PVM-infected mice, but to a higher level in mock/PVM-infected mice (S100a9, Prss22, Fga,
266 Krt17). These genes are also largely involved in inflammation and tissue damage and repair
267 processes.

268 Genes involved in goblet cell metaplasia and mucin production were specifically increased
269 in both RV/PVM and RV/PR8 infected mice compared to the single virus-infected mice at various
270 time points. These included the major gel-forming airway mucins (Muc5ac and Muc5b), a
271 disulfide isomerase (Agr2) required for mucin folding and polymerization, and a chloride channel
272 regulator (Clca1) required for proper hydration of mucus. Additional ion channels (Slc6a20a),
273 aquaporins (Aqp9), and mucus-associated proteins (Itln1) also had increased expression in lungs
274 from RV-treated mice. In addition to the mucin-related genes shared with RV/PR8, RV/PVM
275 infected mice had increased expression of a transcription factor (FoxA3) that promotes goblet cell
276 metaplasia and mucus production. Muc5ac and Clca1 had increased expression in RV-treated mice
277 at all time points (Fig 5).

278 Based on the importance of type I IFN and inflammatory signaling pathways in the
279 pathogenesis of viral infections, we generated heatmaps demonstrating relative gene expression
280 across all groups for genes in the Hallmark Interferon Alpha Response and Inflammatory Response
281 gene sets from MSigDB (44, 45). Overall, IFN-response genes had higher expression in RV/PR8
282 vs. mock/PR8 mice on day 2 and lower expression by day 6 (Fig 6A and S6 Fig). This pattern
283 corresponds with our previous study that demonstrated increased expression of IFN-β only on day
284 2 in RV/PR8 compared to mock/PR8 infected mice (10) and also the lower PR8 gene expression
285 in RV/PR8 infected mice (Fig 4). In contrast, mock/PVM and RV/PVM infected mice had delayed
286 up-regulation of IFN-response genes and mock/PVM infected mice had dramatically higher

287 expression of IFN-response genes compared to RV/PVM on day 4 (Fig 6B and S6 Fig). This
288 pattern was validated by RT-qPCR analysis of IFN-β expression (Fig 8D) and corresponds with
289 the overall delayed PVM-induced gene expression and reduced levels of PVM RNA in RV/PVM
290 infected mice (Fig 4). Inoculation with RV induced expression of a small subset of IFN-response
291 genes (Il7, Ifi27, Lamp3, Cd74, Ifi30, and Lpar6) on day 0, which was maintained in RV/PVM-
292 infected mice on day 2 (Fig 6B). While more variation in gene expression patterns was observed
293 in the inflammatory response gene set, a large number of genes followed the same trends seen for
294 IFN-response genes, i.e., a largely dampened response in RV-treated mice especially at later time
295 points (Fig 6C, 6D and S7 Fig). By day 6, mock/PR8-infected mice had strongly up- and down-
296 regulated expression of inflammatory response genes, while RV/PR8-infected mice had muted
297 changes in expression of these genes (Fig 6C). A large subset of inflammatory response genes had
298 similar patterns as IFN-response genes in mock/PVM and RV/PVM mice, including delayed
299 expression and a muted response in RV-treated mice (Fig 6D). This subset includes important
300 inducers of inflammatory responses such as Nfkb1, Nfkbia, Rela, and Tlr3. Other subsets of genes
301 (e.g., Ccl17 and Ccl22) had early up-regulation in RV-inoculated mice on day 0, which was
302 maintained on day 2 after infection with PVM, and reduced in RV/PVM infected mice on days 4
303 and 6. In contrast with IFN-response genes, subsets of inflammatory response genes had higher
304 expression in RV/PVM compared to mock/PVM infected mice throughout the course of infection.
305 This suggests that, despite low virus levels (Fig 4) and no clinical signs of disease (Fig 1 and S1)
306 and largely muted host gene expression, expression of some host genes is increased in RV/PVM-
307 infected mice.
308
309 **Flow cytometry analysis**

310 Immune cells recruited to the lungs are affected by and contribute to the gene expression
311 signatures seen in whole lung tissues. To analyze differences in immune cell recruitment to the
312 lungs PR8 and PVM infected mice with and without RV pre-treatment, we quantified innate
313 immune cells in the left lobes by flow cytometry at the same time points as our gene expression
314 analyses (Fig 7) and performed regression analyses to identify significant changes over time (S3
315 Table). Total cell counts from mock/PVM- and RV/PVM-infected mice were fairly consistent
316 across all time points, while total cells in mock/PR8 and RV/PR8 infected mice increased by day
317 6 (S8 Fig). CD11b+ was used to differentiate leukocytes from resident lung cell populations.
318 CD11b+ cells accounted for the increase in mock/PR8 and RV/PR8 infected lungs (Fig 7A). In
319 contrast, while CD11b+ cells increased in the lungs of mice infected with mock/PVM, RV/PVM-
320 infected mice had reduced recruitment of these cells on days 4 and 6 (Fig 7E). Neutrophils were
321 gated based on high expression of CD11b and Ly6G and the remaining cells were identified as
322 alveolar macrophages (CD64+/SiglecF+) and interstitial macrophages (CD11b+/CD64+/SiglecF-
323) (S8 Fig) (46, 47).
324 The proportions of neutrophils and interstitial macrophages followed the same trends as
325 total CD11b+ cells in PVM-infected mice, with lower proportions of these cells on days 4 and 6
326 in RV/PVM-infected mice (Fig 7F, 7G). In contrast, interstitial macrophages were increased in
327 RV/PVM, compared to mock/PVM-infected mice, early in infection. This indicates that pre-
328 treatment with RV stimulates early recruitment of CD11b+ cells, specifically interstitial
329 macrophages, while limiting recruitment of inflammatory cells later in infection. PR8-infected
330 mice had similar trends, however the differences between mock/PR8 and RV/PR8 groups were
331 less dramatic (Fig 7B, 7C). Neutrophil numbers were suppressed in RV/PR8-infected mice
332 compared to mock/PR8-infected mice through-out the time course (Fig 7B). The interstitial

333 macrophage proportions in mock/PR8- and RV/PR8-infected mice increased over time similarly
334 to the total CD11b+ populations (Fig 7C). The lower proportions of neutrophils and interstitial
335 macrophages at later time points in RV-treated mice corresponded with mRNA levels for
336 chemokines. This was predominantly the case for neutrophil chemokines Cxcl1 and Cxcl2 and
337 macrophage chemokines Ccl2 and Ccl7 (S9 Fig). These chemokines were generally lower in
338 RV/PR8-infected mice on day 6 and RV/PVM-infected mice on days 4 and 6 compared to
339 mock/PR8- and mock/PVM-infected mice, respectively.

340 There were no clear trends in alveolar macrophage numbers in mock/PR8- and RV/PR8-
341 infected mice (Fig 7D), though their proportions were significantly higher in RV/PVM-infected
342 mice compared to mock/PVM-infected mice on days 4 and 6 (Fig 7H). This is likely due to
343 depletion of alveolar macrophages by PVM infection of these cells (48). A separate flow cytometry
344 antibody panel was used to quantify CD4+ and CD8+ T cells in the lungs. T cell numbers in
345 mock/PR8 and RV/PR8 infected mice increased over time, but the differences between the groups
346 were not significant (Fig 7I, 7J). RV/PVM-infected mice had modest, yet significantly higher
347 numbers of CD4+ and CD8+ T cells compared to mock/PVM-infected mice on day 6 (Fig 7K,
348 7L).

349

350 **IFNAR signaling is required for RV-mediated protection against PR8, but not PVM**

351 To determine whether signaling by type I IFNs is required for RV-mediated reduction in
352 disease severity, we treated mice with IFN-αβ receptor (IFNAR-1) blocking antibody on days -2
353 (with RV inoculation) and 0 (with PR8 or PVM inoculation). Mock/PR8-infected mice had similar
354 weight loss and mortality with anti-IFNAR and control antibody treatments (Fig 8A). In contrast,
355 treatment with anti-IFNAR antibody completely abrogated the dampening effects of RV on the

356 morbidity and mortality of PR8 (Fig 8A). Thus, IFNAR signaling is required for the reduced
357 disease severity observed in RV/PR8-infected mice. Mice that were inoculated with RV alone did
358 not experience weight loss, clinical signs of infection, or mortality over 14 days when treated with
359 either anti-IFNAR or control antibodies (Fig S10). Interestingly, there were no significant
360 differences in weight loss and mortality between anti-IFNAR- and control antibody- treated
361 RV/PVM-infected mice (Fig 8B). Thus, type I IFN signaling is not required for RV-mediated
362 protection against lethal PVM infection.

363 To verify that IFNAR signaling was effectively inhibited in anti-IFNAR treated mice, we
364 analyzed expression of an IFN-induced gene, Mx1, in mock/PVM and RV/PVM infected mice
365 treated with anti-IFNAR or control antibody. Significant inhibition of Mx1 expression was seen
366 through the course of anti-IFNAR treatment (days -1 through 2) with recovery of IFNAR signaling
367 on day 4 after PVM infection (Fig 8C). In agreement with the weight loss and mortality data,
368 inhibition of IFNAR signaling also had no significant effect on the viral load of PVM in
369 mock/PVM or RV/PVM infected mice (Fig 8E).

370

371 **IFN-dependent protection in RV/PR8 infected mice is associated with reduced viral spread,**
372 **neutrophilic inflammation, and histopathology in the lungs.**

373 Type I IFN signaling stimulates multiple downstream responses, including expression of
374 antiviral genes, activation of innate and adaptive responses, and modulation of inflammatory
375 responses. To better understand the role of IFNAR signaling in limiting disease severity in RV/PR8
376 infected mice, we analyzed PR8 replication, immune cell recruitment, and histopathology in
377 RV/PR8-infected mice treated with anti-IFNAR or control antibodies. Anti-IFNAR treated mice
378 had higher levels of PR8 in the lungs on days 2 and 6 than control antibody-treated mice, though

379 the differences were not statistically significant (Fig 9A). Similarly, PR8 antigen was more
380 widespread in the lungs of anti-IFNAR treated mice on days 2 and 6 post-infection (Fig 9B).
381 However, IFNAR signaling did not completely prevent PR8 replication in RV/PR8-infected mice.
382 This is in agreement with similar levels of PR8 RNA (Fig 4), viral loads, and antigen (10) in
383 RV/PR8 infected mice compared to mock/PR8 infected mice. Inhibition of IFNAR signaling also
384 resulted in higher titers of RV in BALF on day -1, with no infectious RV detected in IFNAR
385 inhibited or control animals on day 0 (Fig S10).

386 Mice treated with anti-IFNAR antibody had a slightly higher percentage of neutrophils in
387 the airways compared to mice treated with a control antibody (Fig 9C), however the difference
388 was not statistically significant. Overall inflammation was similar in the lungs of RV/PR8-infected
389 mice treated with anti-IFNAR and control antibodies (Fig 9D). However, immunohistochemical
390 (IHC) staining for a neutrophil-specific protein, Ly6G, indicated that IFNAR signaling limits
391 neutrophilic inflammation in RV/PR8-infected lungs (Fig 9E). Enhanced neutrophilic
392 inflammation in the lung parenchyma of anti-IFNAR treated mice was accompanied by increased
393 infiltration of red blood cells into the alveoli (pulmonary hemorrhage) on day 6 (Fig 9D).
394 Altogether, this suggests that type I IFN signaling plays a role in reducing, but not eliminating,
395 viral replication and curtailing both neutrophil spread within the lungs and pulmonary hemorrhage
396 in RV/PR8-infected mice.

397 In order to evaluate RV-induced recruitment of cells in the airways of mice, we quantified
398 macrophages, neutrophils and lymphocytes in BALF from mice that received mock or RV with or
399 without anti-IFNAR treatment on day 2 after inoculation (day 0 of study). Inoculation with RV
400 did not increase the overall cell counts in BALF, but dramatically changed the composition from

401 predominantly macrophages to neutrophils (Fig 10). Inhibition of IFNAR signaling did not alter
402 cellular recruitment in response to RV infection.
403

404 ## Discussion

405 Previously, we found that inoculation of mice with a mild respiratory viral pathogen, RV
406 or murine coronavirus MHV-1, two days before PR8 provided significant protection against PR8-
407 mediated disease (10). In this study, we expanded these results to show that RV-mediated
408 protection was not specific to PR8, but also provided significant disease protection against a
409 respiratory virus from another viral family, PVM. This is in agreement with other studies showing
410 heterologous immunity by respiratory viral pathogens in mouse models (11-13);(14). Recently,
411 RV has been shown to inhibit replication of influenza A virus and SARS-coronavirus-2 in cultured
412 airway epithelial cells (9, 49). Interference by respiratory viruses within a human host may
413 contribute to reduced disease severity and alter population-level viral dynamics. Coinfection by
414 rhinoviruses has been associated with reduced severity of the 2009 pandemic influenza A virus
415 strain despite similar H1N1 viral loads (50). Conversely, infection with influenza viruses has also
416 been found to reduce the severity of rhinovirus infections (51). Epidemiological studies have
417 suggested that co-circulating viruses, especially rhinoviruses, can inhibit population-level
418 dynamics of other respiratory viruses (49, 50, 52-54). In 2009, introduction of the new pandemic
419 H1N1 strain delayed the circulation of other seasonal respiratory viruses (55). A large study of
420 children with community acquired pneumonia found the incidence of rhinoviruses to be high,
421 however rhinoviruses were found less frequently in combination with other RNA viruses,
422 including influenza and RSV, than would be expected if coinfection were random (3). Similar
423 findings have been reported in adult populations (49). Another large, multi-center study of infants

424 observed significant interference between RSV and RV (56). A prospective study of children
425 found that infection with RV did not affect the likelihood of having an influenza infection the
426 following week, but an influenza infection decreased the chances of having RV the following week
427 (57). In a study of RSV and influenza cases across seven seasons in Israel, they found that when
428 the peak of RSV cases coincided with the influenza peak, the percent RSV positive cases were
429 lower than when the RSV cases peaked prior to influenza (14). While these studies suggest an
430 important role of respiratory viral coinfection in viral pathogenesis and epidemiology, animal
431 models are necessary to understand the interactions between co-infecting viruses and their host
432 that may contribute to these observations.

433 Despite the commonality of RV reducing disease severity of two heterologous lethal
434 viruses in our mouse model, there are differences between the virus combinations in the kinetics
435 of disease and viral replication. Inoculation of mice with RV provided more effective protection
436 against PVM than PR8. RV/PVM infected mice had little to no signs of disease and significantly
437 limited PVM gene expression. In contrast, coinfection by RV prevented mortality, but not
438 morbidity, associated with PR8 infection, and reduced viral gene expression but did not prevent
439 infection by PR8 (10). Further, RV given concurrently with PVM was as effective as when it was
440 given two days before PVM. In contrast, we previously showed that RV was less effective at
441 reducing the severity of PR8 when given concurrently and also exacerbated disease when it was
442 given two days after PR8 (10). We also observed differences in the kinetics of gene expression in
443 response to these virus pairs. Host and viral gene expression changes in response to PVM were
444 delayed compared to PR8, thereby giving a larger window for RV-mediated protection. Thus, RV
445 may be inducing antiviral mechanisms that are more effective against PVM, or different
446 mechanisms may be responsible for inhibiting PVM infection and mediating effective clearance

447 of PR8. In support of the latter, we found that IFNAR signaling was required for RV-mediated
448 reduction in disease severity during PR8, but not PVM, infection.

449 While we do not know if RV replicated in the airways or lungs, intranasal inoculation with
450 a high dose of RV resulted in dramatic up-regulation of host gene expression prior to inoculation
451 with the second, lethal virus. Despite expression of several chemokine and chemokine receptor
452 genes, we did not observe a dramatic increase in immune cells in the lungs of RV- inoculated mice
453 on day 0. Our flow cytometry panel was limited to focus on inflammatory cells (neutrophils and
454 macrophages) and T cells and likely missed other cell types that could be recruited by RV early in
455 infection. Further, by using whole lung for our assays, we may miss populations of cells that are
456 small, but significant, in the airways. Indeed, other studies have found that neutrophils and
457 lymphocytes are increased in the airways of RV-infected mice two days after inoculation (39, 58),
458 which we also detected by analyzing BALF. While the chemokine signaling genes we identified
459 in RV-inoculated mice on day 0 were also increased in single virus infected mice later, early
460 upregulation of immune cell recruitment in RV-treated mice may contribute to early control of
461 infection and reduced disease severity.

462 In contrast to early recruitment of neutrophils, RV-treated mice had reduced numbers of
463 neutrophils and interstitial macrophages later during infection, which could be a result of reduced
464 viral infection and/or direct down-regulation of the inflammatory response. Other studies have
465 shown that rhinoviruses inhibit macrophage responses to bacterial infection and toll-like receptor
466 (TLR) stimulation (59, 60). This down-regulation leads to reduced neutrophil recruitment and
467 activation and results in enhanced bacterial infection. While suppression of TLR signaling is
468 detrimental during a subsequent bacterial infection, it can be protective in the case of respiratory
469 viral infections for which inflammatory responses contribute to disease pathology. Blocking

470 signaling from multiple TLRs (TLR2, TLR4, TLR7, and TLR9) through inhibiting the adaptor
471 protein TIRAP reduces the severity of a lethal PR8 infection in mice (61). Inhibition of TIRAP
472 reduces PR8-induced cytokine production by macrophages and is likely protective by limiting
473 inflammatory responses (61). Similarly, inhibition of TLR2 and TLR4 signaling during PR8
474 infection reduces inflammatory cytokine responses and disease severity (62).

475 Inflammatory responses, particularly by granulocytes, are also associated with disease
476 pathogenesis of PVM infection, independent of viral replication (34, 35). Priming with probiotic
477 bacteria or parasitic infections can reduce the severity of PVM, which corresponds with reduced
478 pulmonary inflammation. When given intranasally on days -14 and -7 prior to, or days 1 and 2
479 after PVM inoculation, *Lactobacillus spp.* prevent lethal viral infection (28, 63, 64). Bacterial
480 priming is associated with reduced production of proinflammatory cytokines and chemokines and
481 inflammatory cell recruitment to the lungs, especially neutrophils (28, 63, 64). Similarly, chronic
482 schistosomiasis protects mice from a lethal PVM infection, which corresponds with up-regulation
483 of mucus secretion pathways (32).

484 We found that RV-treated mice had increased expression of several genes in the mucin
485 production pathway. Muc5ac, the predominant gel-forming mucin in the airways of humans and
486 mice, is produced by goblet cells in the airway epithelium and Clca1 is a chloride channel regulator
487 that is needed for proper mucus hydration. The forkhead transcription factor, FoxA3, induces
488 expression of multiple genes in the mucus production pathway that we found to be concurrently
489 upregulated, including Muc5ac, Muc5b, Agr2, and Itln1 (65). Chen et al. demonstrated increased
490 expression of FoxA3 and Muc5ac and goblet cell metaplasia in the airway epithelium of mice 3
491 days after infection by RV (65), and additional studies have reported up-regulation of Muc5ac
492 mRNA and protein in the lungs and airways of RV-infected mice (39, 65, 66). Influenza A virus

493 strains, including PR8, also induce expression of Muc5ac and mucus secretion (67-69). While
494 stimulation of mucus production can promote pathology in chronic airway diseases such as asthma
495 and COPD, acute mucus production in hosts with healthy airways promotes innate defense against
496 pathogen invasion. Over-expression of Muc5ac in mice has been shown to reduce PR8 infection
497 and neutrophil recruitment (33). Muc5ac also promotes neutrophil transmigration and recruitment
498 (70), thus the reduction in neutrophils seen by Ehre *et al*. may be a consequence of lower viral
499 replication. Muc5ac has also been shown to reduce the severity of PR8 and PVM infections in a
500 parasite coinfection model (32). Production of Muc5ac is induced by multiple inflammatory
501 mediators, including IL-4, IL-13, EGF, and TGF-α, and is enhanced by additional signaling
502 molecules through MAPK-dependent pathways (71). Muc5ac is also upregulated by IFN-β in
503 human bronchial and alveolar epithelial cells and mouse lung tissues, and is dependent on signaling
504 through aryl hydrocarbon receptor (AhR) (72). Thus, upregulation of Muc5ac by RV is likely not
505 prevented by inhibition of IFNAR signaling and thus not sufficient to prevent PR8 lethality. Future
506 studies will address the potential role of mucins in RV-mediated protection against PVM disease.
507 We found dramatic differences in the kinetics of interferon (IFN)-response gene expression
508 in PR8- vs. PVM-infected mice, which corresponded with differences in the requirement of
509 IFNAR signaling in protection against PR8, but not PVM. Although PVM encodes two
510 nonstructural proteins with potent antagonist activity against type I IFN, treatment of mice with
511 type I IFN prior to PVM infection is protective (22). It is possible that the IFN response to RV is
512 not robust enough to account for protection against PVM or multiple, redundant mechanisms may
513 contribute to protection, for example type I and type III IFN (22).
514 Type I IFN signaling is important for immediate antiviral defense mechanisms as well as
515 orchestrating the correct balance of immune cells responding to infection. Others have shown that

516 type I IFN signaling is critical for orchestrating monocyte responses to PR8 infection, which in
517 turn limits neutrophilic inflammation (20). We observed increased numbers of neutrophils in
518 BALF and through-out lung tissues in RV/PR8 coinfected mice that were treated with an IFNAR
519 inhibiting antibody. These findings demonstrate that type I IFN can provide protection during
520 respiratory viral infections that is independent of direct inhibition of viral replication and correlates
521 with reduced neutrophilic inflammation and tissue damage. Type I IFN responses are also
522 important in the activation of T cell-mediated immune responses (73-75). While they did not reach
523 statistical significance, the numbers of CD4+ and CD8+ T cells in the lungs were modestly
524 increased in RV/PR8- compared to mock/PR8-infected mice on day 6. Future studies to evaluate
525 potential functional differences in lung-resident and recruited T cell subsets and their roles in
526 protection will be critical for a complete understanding the type I IFN-dependent mechanisms
527 whereby RV reduces the severity of PR8 infection.
528

529 ## Materials and Methods

530 **Ethics Statement**

531 All mouse procedures were approved by the University of Idaho's Institutional Animal
532 Care and Use Committee, in compliance with the NIH Guide for the Care and Use of Laboratory
533 Animals. Female, 6-7 week-old BALB/c mice were ordered from Invivogen/Envigo and were
534 allowed to acclimatize for 10 days prior to experimentation. All mice were housed in the UI
535 Laboratory Animal Research Facility under 12 hour light/dark cycles, received food and water *ad*
536 *libitum*, and were monitored daily for any signs of distress. Mice were humanely euthanized if they
537 reached endpoints including more than 25% weight loss and/or severe clinical signs of disease.
538

539 **Virus Infections**

540 Viruses used in this study include PVM strain 15 (ATCC VR-25), RV1B strain B632
541 (ATCC VR-1645) and influenza A virus, A/Puerto Rico/8/34 (H1N1; BEI Resources NR-3169).
542 Viruses were grown and titrated by $TCID_{50}$ assays in BHK-21 (PVM), HeLa (RV1B), and MDCK
543 (PR8) cell lines.

544 Mice were anesthetized using isoflurane during intranasal inoculation. RV/PVM timing
545 experiments were performed using groups of seven mice. Mice were either mock-inoculated
546 (PBS/2% FBS) or inoculated with 7.6 x 10^6 $TCID_{50}$ units of RV1B two days before,
547 simultaneously with, or two days after 1.0 x 10^4 $TCID_{50}$ units PVM in 0.05 mL intranasally. Mice
548 were then monitored daily for mortality, weight loss, and clinical signs of disease (ruffled fur,
549 hunched posture, lethargy, and labored breathing). Clinical signs in these four categories were
550 scored on a scale of 0-3 (0-none, 3-severe). Humane euthanasia was performed when mice lost
551 more than 25% of their starting weight or exhibited severe clinical signs of disease. Survival and
552 weight loss data were analyzed with Prism 8.0 (Graphpad) software using Log-rank Mantel-Cox
553 and student's *t*-test corrected for multiple comparisons using the Holm-Sidak method, respectively.

554 RNA-seq and flow cytometry experiments were performed using groups of five mice. Mice
555 were either mock-inoculated (PBS/2% FBS) or inoculated with 7.6 x 10^6 $TCID_{50}$ units RV1B
556 intranasally on day -2. On day 0, mice were either inoculated with ~50 $TCID_{50}$ units of PR8 or 1.0
557 x 10^4 $TCID_{50}$ units of PVM. Mice were euthanized on days 0, 2, 4, and 6 to collect lungs for
558 analyses. Left lobes were used for flow cytometry analysis and right lobes were placed in
559 RNALater for RNA-seq analysis (see below). We consistently see infection in right and left lobes
560 upon intranasal inoculation of PR8 or PVM in 50 uL volumes (S11 Fig).

561 Signaling by interferon alpha receptor 1 (IFNAR1) was inhibited by treating mice with
562 0.05 mg anti-IFNAR1 antibody (MAR1-5A3, Bio X Cell) intranasally on days -2 and 0 with virus
563 or mock inoculations. Antibody of the same isotype (mouse IgG1k, MOPC-21, Bio X Cell) was
564 used as a negative control. Mice were monitored and weighed daily as described above and groups
565 of 5 mice were euthanized at pre-determined time points to quantify viral replication, IFN-induced
566 gene expression, and cellular infiltration.
567
568 **RNA-seq Analysis**
569 RNA was extracted from mouse lung tissue according to the RNeasy Plus with gDNA
570 removal protocol (QIAGEN) and quantified using an HS RNA kit and Fragment Analyzer
571 (Advanced Analytical). The three samples with the highest RNA quality from each group were
572 used for RNA-seq analysis. Stranded RNA libraries were prepared from 4 ug RNA of each sample
573 by UI's IBEST Genomics Resources Core according to KAPA's stranded mRNA-seq (KK8420)
574 library preparation protocol with capture of polyadenylated mRNAs. Libraries were tagged with
575 unique ligation adapters (BioOScientific), amplified, quantified (Qubit and AATI Fragment
576 Analyzer), and pooled at an equimolar ratio. The pooled library was split, pooled with other
577 libraries, and sequenced across 5 lanes of an Illumina HiSeq4000 100bp PE run at University of
578 Oregon's Genomics and Cell Characterization Core. Paired end reads (100 bp) were quality
579 trimmed and filtered using Trimmomatic v0.36 (ILLUMINACLIP:2:20:10, HEADCROP:10,
580 SLIDINGWINDOW:4:15, MINLEN:36) and mapped to the mouse genome (GRCm38/mm10
581 downloaded from UCSC) using TopHat v2.1.1 (r 300) (76, 77). The TopHat alignments were the
582 starting points for two methods of quantifying read counts and four methods of analyzing
583 differential expression. The Cufflinks v2.1.1 package (Cufflinks, Cuffmerge, Cuffdiff) was

584 compared to DE pipelines using HTSeq v0.8.0 (htseq-count -m intersection -nonempty -s reverse
585 -t exon) followed by DESeq2 v1.18.1, and EdgeR 3.18.1 (78, 79). DESeq2 and EdgeR were run
586 within the SARTools wrapper (80). DEGs with adjusted p values below 0.05 were dropped. A text
587 file containing important parameters and code is included in S1 File.

588 *Analysis of viral gene expression*

589 Reads that did not map to the mouse genome were extracted and de-interleaved using
590 BBmaps' reformat script (http://sourceforge.net/projects/bbmap/) to give pair reads for mapping.
591 These reads were aligned to the RV1B (D00239), PR8 (LC120388-LC120395), and PVM
592 (AY729016) genomes using TopHat v2.1.1 and gene coverages were counted using HTseq v0.8.0
593 (see parameters above). Statistical significance was determined using a generalized linear model
594 in R.

595 *DEG function analysis*

596 The DEG lists for each treatment comparison were searched for differentially enriched
597 gene ontologies (GO terms) and KEGG pathways using CompGO (81). CompGO utilizes gene
598 expression level data (as opposed to just gene names) to identify potential functions that differ
599 between treatments. We ran CompGO on DEG lists from each individual method (Cufflinks,
600 EdgeR, DESeq2) and combinations of gene sets to anecdotally look for consistency across
601 methods.

602

603 **RT-qPCR**

604 RNA was extracted from lung tissues using Trizol (Invitrogen) or RNAeasy Plus
605 (QIAGEN) reagents following the manufacturers' protocols. cDNA synthesis was performed
606 using SuperScript IV VILO master mix (Invitrogen) and qPCR was done with PowerUp SYBR

607 Green (Applied Biosystems) using a StepOnePlus real-time instrument (applied Biosystems).
608 Published primer sets were used to quantify PR8 HA (82), PVM SH (83), IFN-β (84), Mx1 (73),
609 GAPDH (85), and β-actin (86). Mx1 and IFN-β C_T values were normalized to GAPDH and the
610 resulting ΔC_T values were normalized to those from mock-inoculated mice and expressed as 2^{-}
611 $^{\Delta\Delta CT}$. C_T values of viral genes were normalized to β-actin and expressed as $2^{-\Delta CT}$.
612

613 **Flow Cytometry**

614 The left lung lobe of each sample was dissociated in RPMI medium containing type IV
615 collagenase (MP Biomedicals) and DNase I (Spectrum) using gentleMACS C tubes according to
616 the manufacturer's recommendations (Miltenyi Biotec). Cells were filtered through a 70 µm
617 strainer and red blood cells were lysed before blocking F_C receptors using anti-CD16/CD32
618 (BioLegend). Cell-specific proteins were labeled with the following antibodies: CD11b-Alexa
619 Fluor 488 (eBiosciences), Ly6G-APC (eBiosciences), CD64-PE (BioLegend), SiglecF-PerCP-
620 Cy5.5 (BD Biosciences), or the appropriate isotype control antibodies. T cell subsets were stained
621 with antibodies against CD3-PerCP-Cy5.5 (eBiosciences), CD8-APC (eBiosciences), and CD4-
622 Alexa Fluor 488 (BioLegend). Stained cells were incubated in BD Stabilizing Fixative (BD
623 Biosciences) and analyzed using a FACS Aria Cytometer (BD Biosciences). Results were analyzed
624 using FlowJo software (Treestar) and gating was performed based on fluorescence-minus-one
625 controls. The gating strategy used to identify neutrophils, alveolar macrophages, and interstitial
626 macrophages is shown in S8 Fig. T cells were gated as CD3+/CD4+ T-helper cells and
627 CD3+/CD8+ cytotoxic T cells.
628

629 **Quantification of Viral Loads**

630 Infectious virus was quantified in homogenized lungs or BALF samples by $TCID_{50}$ assays
631 in HeLa (RV), MDCK (PR8) and BHK21 (PVM) cell lines. We have previously found that the
632 presence of RV in samples does not interfere with titration of PR8 or PVM in MDCK cells or
633 BHK21 cells, respectively (10).
634
635 **Analysis of BALF cells**
636 BALF was collected by tracheal cannulation and lavage with 1 mL PBS twice per sample.
637 Collected cells were counted and spun onto microscope slides in duplicate samples, which were
638 stained with Hema 3 staining solutions (Fisher Scientific). Gridded coverslips and microscopy
639 were used to count at least 300 neutrophils, macrophages and lymphocytes per sample and these
640 counts were used to calculate the percentage of each cell type.
641
642 **Histology and Immunohistochemistry**
643 Lung tissues from two animals per treatment group and time point were processed and
644 stained as previously described (10). Antibodies specific for PR8 hemagglutinin protein (NR-3148,
645 BEI Resources) and Ly6G (1A8, Bio X Cell) were detected with immPACT vector red and
646 immPACT DAB, respectively (Vector Laboratories).
647
648 **Statistical Analyses**
649 We analyzed flow cytometry (Fig 7) and viral read count (Fig 4) data resulting from our
650 experiments to identify time-varying differences between mice infected with PR8 or PVM alone
651 or pre-treated with RV. To this end, we used negative binomial regression on each response
652 variable with an explanatory model that had a main effect of days post-infections, a main effect of

653 treatment, and the interaction between the two main effects. Response variables were the number
654 of CD11b cells, neutrophils, interstitial macrophages, alveolar macrophages, and viral read counts;
655 all response variables were normalized versus total cell count except for viral RNA read count
656 which was normalized against total RNA read count. Due to *a priori* visual investigation of our
657 data, it seemed some of our response variables might be better fit with a quadratic time term.
658 Because of this we fit an alternative model that included an orthogonal polynomial of degree 2 for
659 time. We assessed whether the quadratic model was better than the linear model using a likelihood
660 ratio test and chose the quadratic model if it offered a significant improvement in fit over the
661 simpler linear model. The significance of treatment and time was determined using a type-I
662 ANOVA. To detect differences between treatments at a given time, we also performed *post*
663 *hoc* pairwise comparisons of the modeled mean at our observational time points (days 0, 2, 4, and
664 6) using the emmeans package in R. Supplemental Table 3 provides information on the analyses,
665 including which time model was used, the significance of treatment and time. Significant contrasts
666 are shown in individual figures.

667 Analysis of survival curves, weight loss, viral titers, RT-qPCR, and BALF cell count data
668 were analyzed with Prism 8.0 (Graphpad) software using the methods described in each figure
669 legend.

670

671 **Data Availability**

672 Raw Illumina reads have been deposited in NCBI SRA database under accession numbers
673 SRR7060120-SRR7060117 under project PRJNA453386.

674

675 **Acknowledgements**

676 This study was supported by the National Institutes of Health (NIH) grants P20 GM104420
677 and P20 GM103397. Maricris Naranjo was supported by the REU Summer Program in Molecular
678 and Organismal Evolution, funded by the National Science Foundation (Award #1757826). We
679 thank the Institute for Bioinformatic and Evolutionary Studies (IBEST) Genomics Resources Core
680 and Optical Imaging Core and the laboratory of Dr. Shirley Luckhart for support. We would also
681 like to acknowledge the excellent technical support of Dr. Bhim Thapa and Mr. Kevin Hutchison.
682 The following reagents were obtained through the NIH Biodefense and Emerging Infections
683 Research Resources Repository, NIAID, NIH: Influenza A Virus, A/Puerto Rico/8/34 (H1N1).

684

685 **References**

686 1. Cilla G, Onate E, Perez-Yarza EG, Montes M, Vicente D, Perez-Trallero E. Viruses in community-
687 acquired pneumonia in children aged less than 3 years old: High rate of viral coinfection. Journal of Medical
688 Virology. 2008;80(10):1843-9.
689 2. Goka E, Vallely P, Mutton K, Klapper P. Influenza A viruses dual and multiple infections with
690 other respiratory viruses and risk of hospitalisation and mortality. Influenza Other Respir Viruses.
691 2013;7(6):1079-87.
692 3. Nolan VG, Arnold SR, Bramley AM, Ampofo K, Williams DJ, Grijalva CG, et al. Etiology and
693 Impact of Coinfections in Children Hospitalized With Community-Acquired Pneumonia. J Infect Dis.
694 2018;218(2):179-88.
695 4. Xia W, Shao J, Guo Y, Peng X, Li Z, Hu D. Clinical and CT features in pediatric patients with
696 COVID-19 infection: Different points from adults. Pediatr Pulmonol. 2020;55(5):1169-74.
697 5. Martin ET, Kuypers J, Wald A, Englund JA. Multiple versus single virus respiratory infections:
698 viral load and clinical disease severity in hospitalized children. Influenza and other respiratory viruses.
699 2012;6(1):71-7.
700 6. Kim D, Quinn J, Pinsky B, Shah NH, Brown I. Rates of co-infection between SARS-CoV-2 and
701 other respiratory pathogens. JAMA. 2020;323(20):2085-6.
702 7. Li Z, Chen Zm, Y LDC, Zhan aQ, Li SQ, Cheng J, et al. Coinfection with SARS-CoV-2 and other
703 respiratory pathogens in patients with COVID-19 in Guangzhou, China. Journal of Medical Virology.
704 2020;92(11):2381-3.
705 8. Lansbury L, Lim B, Baskaran V, Lim WS. Co-infections in people with COVID-19: a systematic
706 review and meta-analysis. Journal of Infection. 2020;81(2):266-75.
707 9. Dee K, Goldfarb DM, Haney J, Amat JAR, Herder V, Stewart M, et al. Human rhinovirus infection
708 blocks SARS-CoV-2 replication within the respiratory epithelium: implications for COVID-19
709 epidemiology. The Journal of infectious diseases. 2021;jiab147(https://doi.org/10.1093/infdis/jiab147).
710 10. Gonzalez AJ, Ijezie EC, Balemba OB, Miura TA. Attenuation of Influenza A Virus Disease
711 Severity by Viral Coinfection in a Mouse Model. J Virol. 2018;92(23):pii: e00881-18.
712 11. Hua X, Vijay R, Channappanavar R, Athmer J, Meyerholz DK, Pagedar N, et al. Nasal priming by
713 a murine coronavirus provides protective immunity against lethal heterologous virus pneumonia. JCI
714 Insight. 2018;3(11).

715 12. Laurie KL, Guarnaccia TA, Carolan LA, Yan AW, Aban M, Petrie S, et al. Interval Between
716 Infections and Viral Hierarchy Are Determinants of Viral Interference Following Influenza Virus Infection
717 in a Ferret Model. J Infect Dis. 2015;212(11):1701-10.
718 13. Chan KF, Carolan LA, Korenkov D, Druce J, McCaw J, Reading PC, et al. Investigating Viral
719 Interference Between Influenza A Virus and Human Respiratory Syncytial Virus in a Ferret Model of
720 Infection. J Infect Dis. 2018;218(3):406-17.
721 14. Drori Y, Jacob-Hirsch J, Pando R, Glatman-Freedman A, Friedman N, Mendelson E, et al.
722 Influenza A virus inhibits RSV infection via a two-wave expression of IFIT proteins. Viruses.
723 2020;12(10):1171.
724 15. Dyer KD, Garcia-Crespo KE, Glineur S, Domachowske JB, Rosenberg HF. The Pneumonia Virus
725 of Mice (PVM) model of acute respiratory infection. Viruses. 2012;4(12):3494-510.
726 16. Easton AJ, Domachowske JB, Rosenberg HF. Animal pneumoviruses: molecular genetics and
727 pathogenesis. Clin Microbiol Rev. 2004;17(2):390-412.
728 17. Habibi MS, Thwaites RS, Chang M, Jozwik A, Paras A, Kirsebom F, et al. Neutrophilic
729 inflammation in the respiratory mucosa predisposes to RSV infection. Science. 2020;370(6513):eaba9301.
730 18. Garvey TL, Dyer KD, Ellis JA, Bonville CA, Foster B, Prussin C, et al. Inflammatory responses to
731 pneumovirus infection in IFN-alpha beta R gene-deleted mice. J Immunol. 2005;175(7):4735-44.
732 19. Walsh KB, Teijaro JR, Brock LG, Fremgen DM, Collins PL, Rosen H, et al. Animal model of
733 respiratory syncytial virus: CD8+ T cells cause a cytokine storm that is chemically tractable by sphingosine-
734 1-phosphate 1 receptor agonist therapy. J Virol. 2014;88(11):6281-93.
735 20. Seo SU, Kwon HJ, Ko HJ, Byun YH, Seong BL, Uematsu S, et al. Type I interferon signaling
736 regulates Ly6C(hi) monocytes and neutrophils during acute viral pneumonia in mice. PLoS Pathog.
737 2011;7(2):e1001304.
738 21. Stifter SA, Bhattacharyya N, Pillay R, Florido M, Triccas JA, Britton WJ, et al. Functional Interplay
739 between Type I and II Interferons Is Essential to Limit Influenza A Virus-Induced Tissue Inflammation.
740 PLoS Pathog. 2016;12(1):e1005378.
741 22. Heinze B, Frey S, Mordstein M, Schmitt-Graff A, Ehl S, Buchholz UJ, et al. Both nonstructural
742 proteins NS1 and NS2 of pneumonia virus of mice are inhibitors of the interferon type I and type III
743 responses in vivo. J Virol. 2011;85(9):4071-84.
744 23. Mordstein M, Kochs G, Dumoutier L, Renauld JC, Paludan SR, Klucher K, et al. Interferon-lambda
745 contributes to innate immunity of mice against influenza A virus but not against hepatotropic viruses. PLoS
746 Pathog. 2008;4(9):e1000151.
747 24. Rigaux P, Killoran KE, Qiu Z, Rosenberg HF. Depletion of alveolar macrophages prolongs survival
748 in response to acute pneumovirus infection. Virology. 2011.
749 25. Cardani A, Boulton A, Kim TS, Braciale TJ. Alveolar Macrophages Prevent Lethal Influenza
750 Pneumonia By Inhibiting Infection Of Type-1 Alveolar Epithelial Cells. PLoS Pathog.
751 2017;13(1):e1006140.
752 26. Davidson S, Kaiko G, Loh Z, Lalwani A, Zhang V, Spann K, et al. Plasmacytoid dendritic cells
753 promote host defense against acute pneumovirus infection via the TLR7-MyD88-dependent signaling
754 pathway. J Immunol. 2011;186(10):5938-48.
755 27. Wolf AI, Buehler D, Hensley SE, Cavanagh LL, Wherry EJ, Kastner P, et al. Plasmacytoid
756 dendritic cells are dispensable during primary influenza virus infection. J Immunol. 2009;182(2):871-9.
757 28. Percopo CM, Ma M, Brenner TA, Krumholz JO, Break TJ, Laky K, et al. Critical Adverse Impact
758 of IL-6 in Acute Pneumovirus Infection. J Immunol. 2019;202(3):871-82.
759 29. Pyle CJ, Uwadiae FI, Swieboda DP, Harker JA. Early IL-6 signalling promotes IL-27 dependent
760 maturation of regulatory T cells in the lungs and resolution of viral immunopathology. PLoS Pathog.
761 2017;13(9):e1006640.
762 30. Yang ML, Wang CT, Yang SJ, Leu CH, Chen SH, Wu CL, et al. IL-6 ameliorates acute lung injury
763 in influenza virus infection. Sci Rep. 2017;7:43829.

764 31. Martinez EC, Garg R, Shrivastava P, Gomis S, van Drunen Littel-van den Hurk S. Intranasal
765 treatment with a novel immunomodulator mediates innate immune protection against lethal pneumonia
766 virus of mice. Antiviral Res. 2016;135:108-19.
767 32. Scheer S, Krempl C, Kallfass C, Frey S, Jakob T, Mouahid G, et al. S. mansoni bolsters anti-viral
768 immunity in the murine respiratory tract. PLoS One. 2014;9(11):e112469.
769 33. Ehre C, Worthington EN, Liesman RM, Grubb BR, Barbier D, O'Neal WK, et al. Overexpressing
770 mouse model demonstrates the protective role of Muc5ac in the lungs. Proc Natl Acad Sci U S A.
771 2012;109(41):16528-33.
772 34. Bonville CA, Easton AJ, Rosenberg HF, Domachowske JB. Altered pathogenesis of severe
773 pneumovirus infection in response to combined antiviral and specific immunomodulatory agents. J Virol.
774 2003;77(2):1237-44.
775 35. Bonville CA, Lau VK, DeLeon JM, Gao JL, Easton AJ, Rosenberg HF, et al. Functional
776 antagonism of chemokine receptor CCR1 reduces mortality in acute pneumovirus infection in vivo. J Virol.
777 2004;78(15):7984-9.
778 36. Lin KL, Sweeney S, Kang BD, Ramsburg E, Gunn MD. CCR2-antagonist prophylaxis reduces
779 pulmonary immune pathology and markedly improves survival during influenza infection. J Immunol.
780 2011;186(1):508-15.
781 37. Ichikawa A, Kuba K, Morita M, Chida S, Tezuka H, Hara H, et al. CXCL10-CXCR3 enhances the
782 development of neutrophil-mediated fulminant lung injury of viral and nonviral origin. Am J Respir Crit
783 Care Med. 2013;187(1):65-77.
784 38. Buchholz UJ, Ward JM, Lamirande EW, Heinze B, Krempl CD, Collins PL. Deletion of
785 nonstructural proteins NS1 and NS2 from pneumonia virus of mice attenuates viral replication and reduces
786 pulmonary cytokine expression and disease. J Virol. 2009;83(4):1969-80.
787 39. Bartlett NW, Walton RP, Edwards MR, Aniscenko J, Caramori G, Zhu J, et al. Mouse models of
788 rhinovirus-induced disease and exacerbation of allergic airway inflammation. Nat Med. 2008;14(2):199-
789 204.
790 40. Kebaabetswe LP, Haick AK, Gritsenko MA, Fillmore TL, Chu RK, Purvine SO, et al. Proteomic
791 analysis reveals down-regulation of surfactant protein B in murine type II pneumocytes infected with
792 influenza A virus. Virology. 2015;483:96-107.
793 41. Kummer S, Flottmann M, Schwanhausser B, Sieben C, Veit M, Selbach M, et al. Alteration of
794 protein levels during influenza virus H1N1 infection in host cells: a proteomic survey of host and virus
795 reveals differential dynamics. PLoS One. 2014;9(4):e94257.
796 42. Fabozzi G, Oler AJ, Liu P, Chen Y, Mindaye S, Dolan MA, et al. Strand-Specific Dual RNA
797 Sequencing of Bronchial Epithelial Cells Infected with Influenza A/H3N2 Viruses Reveals Splicing of
798 Gene Segment 6 and Novel Host-Virus Interactions. J Virol. 2018;92(17).
799 43. Collins PL, Fearns R, Graham BS. Respiratory syncytial virus: virology, reverse genetics, and
800 pathogenesis of disease. Curr Top Microbiol Immunol. 2013;372:3-38.
801 44. Subramanian A, Tamayo P, Mootha VK, Mukherjee S, Ebert BL, Gillette MA, et al. Gene set
802 enrichment analysis: a knowledge-based approach for interpreting genome-wide expression profiles. Proc
803 Natl Acad Sci U S A. 2005;102(43):15545-50.
804 45. Liberzon A, Birger C, Thorvaldsdottir H, Ghandi M, Mesirov JP, Tamayo P. The Molecular
805 Signatures Database (MSigDB) hallmark gene set collection. Cell Syst. 2015;1(6):417-25.
806 46. Misharin AV, Morales-Nebreda L, Mutlu GM, Budinger GR, Perlman H. Flow cytometric analysis
807 of macrophages and dendritic cell subsets in the mouse lung. Am J Respir Cell Mol Biol. 2013;49(4):503-
808 10.
809 47. Gibbings SL, Thomas SM, Atif SM, McCubbrey AL, Desch AN, Danhorn T, et al. Three Unique
810 Interstitial Macrophages in the Murine Lung at Steady State. Am J Respir Cell Mol Biol. 2017;57(1):66-
811 76.
812 48. Dyer KD, Drummond RA, Rice TA, Percopo CM, Brenner TA, Barisas DA, et al. Priming of the
813 Respiratory Tract with Immunobiotic Lactobacillus plantarum Limits Infection of Alveolar Macrophages
814 with Recombinant Pneumonia Virus of Mice (rK2-PVM). J Virol. 2015;90(2):979-91.

815 49. Wu A, Mihaylova VT, Landry ML, Foxman EF. Interference between rhinovirus and influenza A
816 virus: a clinical data analysis and experimental infection study. Lancet Microbe. 2020;1(6):e254-e62.
817 50. Esper FP, Spahlinger T, Zhou L. Rate and influence of respiratory virus co-infection on pandemic
818 (H1N1) influenza disease. J Infect. 2011;63(4):260-6.
819 51. Aberle JH, Aberle SW, Pracher E, Hutter HP, Kundi M, Popow-Kraupp T. Single versus dual
820 respiratory virus infections in hospitalized infants: impact on clinical course of disease and interferon-
821 gamma response. Pediatr Infect Dis J. 2005;24(7):605-10.
822 52. Greer RM, McErlean P, Arden KE, Faux CE, Nitsche A, Lambert SB, et al. Do rhinoviruses reduce
823 the probability of viral co-detection during acute respiratory tract infections? J Clin Virol. 2009;45(1):10-
824 5.
825 53. Anestad G, Nordbo SA. Virus interference. Did rhinoviruses activity hamper the progress of the
826 2009 influenza A (H1N1) pandemic in Norway? Med Hypotheses. 2011;77(6):1132-4.
827 54. Casalegno JS, Ottmann M, Duchamp MB, Escuret V, Billaud G, Frobert E, et al. Rhinoviruses
828 delayed the circulation of the pandemic influenza A (H1N1) 2009 virus in France. Clin Microbiol Infect.
829 2010;16(4):326-9.
830 55. Grondahl B, Ankermann T, von Bismarck P, Rockahr S, Kowalzik F, Gehring S, et al. The 2009
831 pandemic influenza A(H1N1) coincides with changes in the epidemiology of other viral pathogens causing
832 acute respiraotry tract infections in children. Infection. 2014;42:303-8.
833 56. Achten NB, Wu P, Bont L, Blanken MO, Gebretsadik T, Chappell JD, et al. Interference Between
834 Respiratory Syncytial Virus and Human Rhinovirus Infection in Infancy. J Infect Dis. 2017;215(7):1102-
835 6.
836 57. Kloepfer KM, Olenec JP, Lee WM, Liu G, Vrtis RF, Roberg KA, et al. Increased H1N1 infection
837 rate in children with asthma. Am J Respir Crit Care Med. 2012;185(12):1275-9.
838 58. Ganesan S, Pham D, Jing Y, Farazuddin M, Hudy MH, Unger B, et al. TLR2 Activation Limits
839 Rhinovirus-Stimulated CXCL-10 by Attenuating IRAK-1-Dependent IL-33 Receptor Signaling in Human
840 Bronchial Epithelial Cells. J Immunol. 2016;197(6):2409-20.
841 59. Unger BL, Faris AN, Ganesan S, Comstock AT, Hershenson MB, Sajjan US. Rhinovirus attenuates
842 non-typeable Hemophilus influenzae-stimulated IL-8 responses via TLR2-dependent degradation of IRAK-
843 1. PLoS Pathog. 2012;8(10):e1002969.
844 60. Oliver BG, Lim S, Wark P, Laza-Stanca V, King N, Black JL, et al. Rhinovirus exposure impairs
845 immune responses to bacterial products in human alveolar macrophages. Thorax. 2008;63(6):519-25.
846 61. Piao W, Shirey KA, Ru LW, Lai W, Szmacinski H, Snyder GA, et al. A Decoy Peptide that Disrupts
847 TIRAP Recruitment to TLRs Is Protective in a Murine Model of Influenza. Cell Rep. 2015;11(12):1941-
848 52.
849 62. Prantner D, Shirey KA, Lai W, Lu W, Cole AM, Vogel SN, et al. The theta-defensin retrocyclin
850 101 inhibits TLR4- and TLR2-dependent signaling and protects mice against influenza infection. J Leukoc
851 Biol. 2017;102(4):1103-13.
852 63. Gabryszewski SJ, Bachar O, Dyer KD, Percopo CM, Killoran KE, Domachowske JB, et al.
853 Lactobacillus-mediated priming of the respiratory mucosa protects against lethal pneumovirus infection. J
854 Immunol. 2011;186(2):1151-61.
855 64. Percopo CM, Rice TA, Brenner TA, Dyer KD, Luo JL, Kanakabandi K, et al. Immunobiotic
856 Lactobacillus administered post-exposure averts the lethal sequelae of respiratory virus infection. Antiviral
857 Res. 2015;121:109-19.
858 65. Chen G, Korfhagen TR, Karp CL, Impey S, Xu Y, Randell SH, et al. Foxa3 induces goblet cell
859 metaplasia and inhibits innate antiviral immunity. Am J Respir Crit Care Med. 2014;189(3):301-13.
860 66. Zhu L, Lee PK, Lee WM, Zhao Y, Yu D, Chen Y. Rhinovirus-induced major airway mucin
861 production involves a novel TLR3-EGFR-dependent pathway. Am J Respir Cell Mol Biol. 2009;40(5):610-
862 9.
863 67. Barbier D, Garcia-Verdugo I, Pothlichet J, Khazen R, Descamps D, Rousseau K, et al. Influenza A
864 induces the major secreted airway mucin MUC5AC in a protease-EGFR-extracellular regulated kinase-
865 Sp1-dependent pathway. Am J Respir Cell Mol Biol. 2012;47(2):149-57.

866 68. Siegel SJ, Roche AM, Weiser JN. Influenza promotes pneumococcal growth during coinfection by
867 providing host sialylated substrates as a nutrient source. Cell Host Microbe. 2014;16(1):55-67.
868 69. Buchweitz JP, Harkema JR, Kaminski NE. Time-dependent airway epithelial and inflammatory
869 cell responses induced by influenza virus A/PR/8/34 in C57BL/6 mice. Toxicol Pathol. 2007;35(3):424-35.
870 70. Koeppen M, McNamee EN, Brodsky KS, Aherne CM, Faigle M, Downey GP, et al. Detrimental
871 role of the airway mucin Muc5ac during ventilator-induced lung injury. Mucosal Immunol. 2013;6(4):762-
872 75.
873 71. Takeyama K, Dabbagh K, Lee H-M, Agusti C, Lausier JA, Ueki IF, et al. Epidermal growth factor
874 system regulates mucin production in airways. Proc of the National Academy of Sciences of the United
875 States of America. 1999;96(6):3081-6.
876 72. Liu Y, Lv J, Liu J, Li MC, Xie J, Lv Q, et al. Mucus production stimulated by IFN-AhR signaling
877 triggers hypoxia of COVID-19. Cell Research. 2020;30:1078-87.
878 73. Moltedo B, Li W, Yount JS, Moran TM. Unique type I interferon responses determine the
879 functional fate of migratory lung dendritic cells during influenza virus infection. PLoS Pathog.
880 2011;7(11):e1002345.
881 74. Kolumam GA, Thomas S, Thompson LJ, Sprent J, Murali-Krishna K. Type I interferons act directly
882 on CD8 T cells to allow clonal expansion and memory formation in response to viral infection. Journal of
883 Experimental Medicine. 2005;202(5):637-50.
884 75. Welsh RM, Bahl K, Marshall HD, Urban SL. Type 1 interferons and antiviral CD8 T-cell
885 responses. PLoS Pathog. 2012;8(1):e1002352.
886 76. Bolger AM, Lohse M, Usadel B. Trimmomatic: a flexible trimmer for Illumina sequence data.
887 Bioinformatics. 2014;30(15):2114-20.
888 77. Kim D, Pertea G, Trapnell C, Pimentel H, Kelley R, Salzberg S. TopHat2: accurate alignment of
889 transcriptomes in the presence of insertions, deletions and gene fusions. Genome Biol. 2013;14(4).
890 78. Trapnell C, Williams B, Pertea G, Mortazavi A, Kwan G, Baren Jv, et al. Transcript assembly and
891 quantification by RNA-Seq reveals unannotated transcripts and isoform switching during cell
892 differentiation. Nature Biotechnology. 2010.
893 79. Anders S, Pyl PT, Huber W. HTSeq—a Python framework to work with high-throughput
894 sequencing data. Bioinformatics. 2015;31(2):166-9.
895 80. Varet H, Brillet-Guéguen L, Coppee J-Y, Dillies M-A. SARTools: A DESeq2- and EdgeR-Based
896 R Pipeline for Comprehensive Differential Analysis of RNA-Seq Data. PLoS One. 2016.
897 81. Waardenberg AJ, Bassett SD, Bouveret R, Harvey RP. CompGO: an R package for comparing and
898 visualizing Gene Ontology enrichment differences between DNA binding experiments. BMC
899 Bioinformatics. 2015;16:275.
900 82. Li H, Bradley KC, Long JS, Frise R, Ashcroft JW, Hartgroves LC, et al. Internal genes of a highly
901 pathogenic H5N1 influenza virus determine high viral replication in myeloid cells and severe outcome of
902 infection in mice. PLoS Pathog. 2018;14(1):e1006821.
903 83. Cortjens B, Lutter R, Boon L, Bem RA, van Woensel JB. Pneumovirus-Induced Lung Disease in
904 Mice Is Independent of Neutrophil-Driven Inflammation. PLoS One. 2016;11(12):e0168779.
905 84. Sommereyns C, Paul S, Staeheli P, Michiels T. IFN-lambda (IFN-lambda) is expressed in a tissue-
906 dependent fashion and primarily acts on epithelial cells in vivo. PLoS Pathog. 2008;4(3):e1000017.
907 85. Jones PH, Mehta HV, Maric M, Roller RJ, Okeoma CM. Bone marrow stromal cell antigen 2 (BST-
908 2) restricts mouse mammary tumor virus (MMTV) replication in vivo. Retrovirology. 2012;9:10.
909 86. Kebaabetswe LP, Haick AK, Miura TA. Differentiated phenotypes of primary murine alveolar
910 epithelial cells and their susceptibility to infection by respiratory viruses. Virus Res. 2013;175(2):110-9.
911

912

913 **Supporting Information**

914 **Supplemental Table 1** provides raw read counts (mean of the three replicates and normalized to
915 library size) and log2 fold change values for genes that had statistically significant differences in
916 expression between each comparison.
917
918 **Supplemental Table 2** provides statistically significant GO terms for each comparison.
919
920 **Supplemental Table 3** provides a summary of results from negative binomial regression analyses
921 of viral read count and flow cytometry data.
922
923 **S1 Fig. Weight loss of mice used in the RNA-seq and flow cytometry experiments.** Mice were
924 inoculated intranasally with saline (mock) or RV on day -2 and PR8 or PVM on day 0. Weight
925 was recorded daily for all mice until the pre-determined time points. Days -2 through 2, N=15 per
926 group; days 3 through 4, N=10 per group; days 5 through 6, N= 5 per group.
927
928 **S2 Fig. Read coverage of individual viral genes.** The proportion of reads mapping to each viral
929 gene is shown for mice infected with PR8 or PVM.
930
931 **S3 Fig. Heatmap of mock/PR8 vs. RV/PR8 unique genes.** Expression of genes that are
932 significantly different between mock/PR8 and RV/PR8 infected mice that are not significant
933 between mock/PVM and RV/PVM infected mice. Colors represent Z-scores for individual genes
934 across infections and time points as described for Fig 6.
935

936 **S4 Fig. Heatmap of mock/PVM vs. RV/PVM unique genes.** Expression of genes that are
937 significantly different between mock/PVM and RV/PVM infected mice that are not significant
938 between mock/PR8 and RV/PR8 infected mice. Colors represent Z-scores for individual genes
939 across infections and time points as described for Fig 6.
940
941 **S5 Fig. Heatmap of differentially expressed genes shared by RV-treated mice.** Expression of
942 genes that are significantly different between mock/PVM and RV/PVM infected mice that are also
943 significant between mock/PR8 and RV/PR8 infected mice. Colors represent Z-scores for
944 individual genes across infections and time points as described for Fig 6.
945
946 **S6 Fig. Heatmaps of MSigDB Hallmark Interferon Alpha Response gene set shown in Figure**
947 **6, including gene names.** See Fig 6 legend for details.
948
949 **S7 Fig. Heatmaps of MSigDB Hallmark Inflammatory Response gene set shown in Figure 6,**
950 **including gene names.** See Fig 6 legend for details.
951
952 **S8 Fig. Total cell counts and gating strategy for flow cytometry.** Left lungs were processed for
953 flow cytometry staining with antibodies against CD11b, Ly6G, CD64, and Siglec F. Total cell
954 counts for all samples and representative plots showing the gating strategy to identify neutrophils,
955 alveolar macrophages, and interstitial macrophages are shown.
956

957 **S9 Fig. RNA-seq data showing chemokine gene expression related to innate inflammatory**
958 **cell recruitment.** Expression of neutrophil and monocyte/macrophage specific chemokine genes
959 from the RNA-seq analysis are shown as Log2 fold change vs. mock-inoculated mice.
960
961 **S10 Fig. Anti-IFNAR treatment of RV-inoculated mice.** Nine mice per group were inoculated
962 intranasally with 7.6 x 10^6 $TCID_{50}$ units of RV on day -2 and received a mock inoculation of buffer
963 on day 0. Mice received either anti-IFNAR or control antibody with the inoculations on days -2
964 and 0. Five mice per group were monitored daily for survival and weight loss. RV was titrated
965 from homogenized lung and BALF samples on days -1 and 0 from 4 mice per group by $TCID_{50}$
966 assay.
967
968 **S11 Fig. Comparison of infection levels in right and left lobes.** Mice were inoculated with
969 mock/PR8 or RV/PR8 as described in materials and methods. RT-qPCR was performed on RNA
970 isolated from right or left lobes of individual mice on day 4 after PR8 inoculation. Microscopic
971 images are shown from serial imaging of lung tissue sections from a mock/PR8-infected mice on
972 day 4 of infection stained for HA antigen visualized with impact red. Images are representative of
973 at least 3 mice.
974

975 ## Figure Legends

976 **Fig 1. Inoculation with RV reduces the severity of PVM infection.** Groups of 7 BALB/c mice
977 were either mock-inoculated (mock/PVM) or inoculated intranasally with 7.6 x 10^6 $TCID_{50}$ units
978 of RV two days before (RV/PVM), simultaneously with (RV+PVM), or two days after (PVM/RV)
979 1.0x10^4 $TCID_{50}$ units of PVM. Mice were monitored daily for (A) mortality and (B) weight loss.

980 Data are representative of two independent experiments. Statistical significance compared to
981 mock/PVM was determined by (A) Log-rank Mantel-Cox test and (B) student's t-test corrected for
982 multiple comparisons using the Holm-Sidak method. P-value *p≤0.05, **p≤0.005, ***p≤0.001.
983
984 **Fig 2**. **Experimental outline of transcriptome study.** Mice were inoculated with RV or saline
985 (mock) two days before challenge with PR8 or PVM. RNA was extracted from lung tissue from
986 three mice per group on day 0 for mock and RV treated controls and days 2, 4, and 6 for mice
987 receiving PR8 or PVM on day 0 and analyzed by RNA-seq.
988
989 **Fig 3. Patterns of mouse gene expression in lungs upon infection with and without RV pre-**
990 **treatment.** (A) Principal component analysis of RNA-seq data shows that the greatest variance in
991 gene expression is primarily due to time since infection. The largest distances in single virus-
992 infected vs. RV-treated groups are mock/PVM vs. RV/PVM on day 4 and mock/PR8 vs. RV/PR8
993 on day 6. (B) Volcano plot showing gene expression changes between mock-inoculated and RV-
994 inoculated mice 2 days post-infection. Only DEGs identified by edgeR, DESeq2, and Cufflinks
995 were considered significant (red points). (C) The scatter plots show the log2 fold change values of
996 all genes compared to mock-inoculated mice on day 0. Genes upregulated in RV-treated compared
997 to the single-virus infected mice are colored green. Down-regulated genes are colored purple. (D)
998 Numbers of DEGs in all pairwise comparisons. The number of genes upregulated in the infected
999 (versus mock) or RV-treated (versus mock or single) mice are shown in green. Downregulated
1000 genes are shown in purple. See Supplemental Table 1 for lists of gene names and log2 fold change
1001 values.
1002

1003 **Fig 4. Viral gene expression in single virus-infected and RV-treated mouse lungs.** (A) RNA-
1004 seq quantification of viral mRNAs. For each group, the three replicates are shown with box plots
1005 indicating the quantile values of percent non-mouse reads mapped to viral genomes. Asterisks
1006 indicate significantly different treatment pairs as determined by a generalized linear model, see
1007 Supplemental Table 3. P-value *$p<0.05$, **$p<0.01$, ***$p\leq0.001$. (B) RT-qPCR analysis of viral
1008 RNAs. Replicates from individual mice are shown with the mean and standard error indicated and
1009 is representative of at least two replicate assays. Statistical significance between single virus-
1010 infected and RV-treated mice at each time point was determined using unpaired t-tests corrected
1011 for multiple comparisons using the Holm-Sidak method. ***$p\leq0.001$.
1012
1013 **Fig 5. Mucin-related genes have increased expression in RV-inoculated mice across all time**
1014 **points.** Log2 fold change values compared to mock day 0 are shown for mucin 5ac (Muc5ac) and
1015 chloride channel accessory 1 (Clca1) genes, which are required for mucus production and
1016 hydration, respectively.
1017
1018 **Fig 6. Expression of MSigDB Hallmark Interferon Alpha Response and Inflammatory**
1019 **Response gene sets.** Heatmaps of Hallmark Interferon Alpha Response genes showing the relative
1020 expression (Z-scores) of genes for the (A) PR8 or (B) PVM infection RNA-seq time course.
1021 Heatmaps of Hallmark Inflammatory Response genes showing the relative expression (Z-scores)
1022 of genes for the (C) PR8 or (D) PVM infection RNA-seq time course. All heatmaps represent
1023 DESeq2 normalized counts where each row represents an individual gene. The genes were ordered
1024 by hierarchical clustering, which is shown on the left side of each heatmap. The colors (blue <
1025 white < red) represent the Z-score and a more intense color indicates a lower (blue) or higher (red)

1026 relative expression of that gene in that condition. Fully labeled heatmaps can be found in S6 and
1027 S7 Fig.
1028
1029 **Fig 7. Flow cytometry analysis of innate immune cell populations in the lungs upon viral**
1030 **infection and RV-treatment.** Mice were inoculated with mock or RV on day -2 and PR8 (A-D,
1031 I, J) or PVM (E-H, K, L) on day 0, followed by analysis of specific cell populations in lung
1032 homogenates by flow cytometry, including total CD11b+ cell counts (A, E), percentages of
1033 $CD11b^{hi}/Ly6G^{hi}$ neutrophils (B, F), CD11b+/CD64+/SiglecF-/Ly6G- interstitial macrophages (C,
1034 B), and CD64+/SiglecF+/Ly6G- alveolar macrophages (D, H), and total numbers of CD3+/CD4+
1035 (I, K) and CD3+/CD8+ (J, L) T cells. Asterisks indicate significantly different treatment pairs, see
1036 Supplemental Table 3. P-value *$p<0.05$, **$p<0.01$, ***$p\leq0.001$.
1037
1038 **Fig 8. IFNAR signaling is required for RV-mediated protection in RV/PR8, but not**
1039 **RV/PVM, infected mice.** Mice were treated with anti-IFNAR or an isotype control (Ctl) antibody
1040 (Ab) intranasally with viral inocula (mock or RV on day -2 and PR8 (A) or PVM (B-E) on day 0).
1041 Animal weights and survival were monitored in five mice per group for 14 days after inoculation
1042 with (A) PR8 or (B) PVM. Significant differences in survival between IFNAR Ab- vs. Ctl Ab-
1043 treated mice were determined using survival curve analysis by log-rank Mantel-Cox test. *$p<0.05$,
1044 ns=not significant, $p>0.05$. (C) Expression of IFN-induced gene, Mx1, was monitored to evaluate
1045 the effectiveness of IFNAR Ab treatment in mock/PVM and RV/PVM infected mice. Data shown
1046 are means and standard error of 4-5 mice per group and are representative of two replicate assays.
1047 (D) IFN-β RNA was quantified by RT-qPCR in 5 animals per group in mock/PVM and RV/PVM
1048 infected mice without antibody treatment. Data shown are means with standard error and are

1049 representative of two assays. (E) PVM titers in BALF were quantified by $TCID_{50}$ assays. Data
1050 shown are from individual animals with the geometric means and standard deviations indicated.
1051 Statistical significance between groups within each time point was determined by unpaired t-tests
1052 corrected for multiple comparison by the Holm-Sidak method. **$p<0.01$, ***$p<0.001$.
1053
1054 **Fig 9. IFNAR-dependent protection in RV/PR8 infected mice is associated with reduced viral**
1055 **spread, neutrophilic inflammation, and histopathology in lungs.** Mice were treated and
1056 infected as described in Fig. 8 legend. (A) PR8 was quantified in homogenized lungs by $TCID_{50}$
1057 assays. Data shown are from five individual mice per group with geometric mean and standard
1058 deviation indicated. Statistical significance between Ctl Ab and IFNAR Ab treated mice was
1059 determined using unpaired t-tests corrected for multiple comparisons using the Holm-Sidak
1060 method, and was not significant ($p>0.05$). (B) Viral antigen in lung tissues was visualized by IHC
1061 using antibody against PR8 HA protein followed by alkaline phosphatase with impact red
1062 substrate. (C) Cytospins from BALF were stained with HEMA 3 to identify airway neutrophils.
1063 At least 300 total cells were counted from duplicate cytospins and the percent neutrophils was
1064 calculated. Data shown are from individual mice with mean and standard error indicated. Statistical
1065 significance between Ctl Ab and IFNAR Ab treated mice was determined using unpaired t-tests
1066 corrected for multiple comparisons using the Holm-Sidak method, and was not significant
1067 ($p>0.05$). (D) Histopathology in lung tissues was visualized by hematoxylin & eosin staining on
1068 day 6 after PR8 infection. Arrows indicate examples of pulmonary hemorrhage. (E) Neutrophils
1069 in lung tissues were visualized by IHC using antibody against Ly6G followed by horseradish
1070 peroxidase and impact DAB substrate. Images in B, D, and E are representative of two mice per
1071 group and time point.

1072

1073 **Fig 10. Airway cellular response to RV inoculation.** Cytospins from BALF were stained with
1074 HEMA 3 to identify airway macrophages, neutrophils, and lymphocytes. At least 300 total cells
1075 were counted from duplicate cytospins for each sample to determine the percentage of each cell
1076 type. Total cells were counted in the BALF samples prior to cytospin preparation. Data shown are
1077 means and standard errors from 5 mice per group. Statistical significance between groups was
1078 determined using unpaired t-tests corrected for multiple comparisons using the Holm-Sidak
1079 method, ***p<0.001.

1080 **Figure 1.**

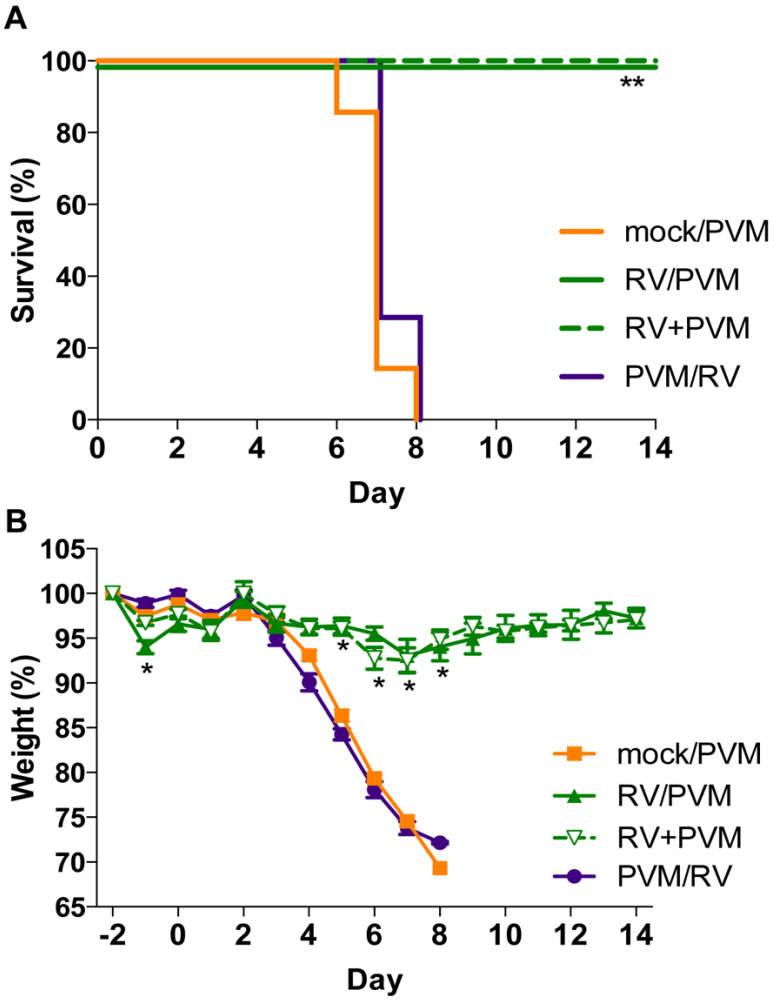

1081

1082 **Figure 2.**

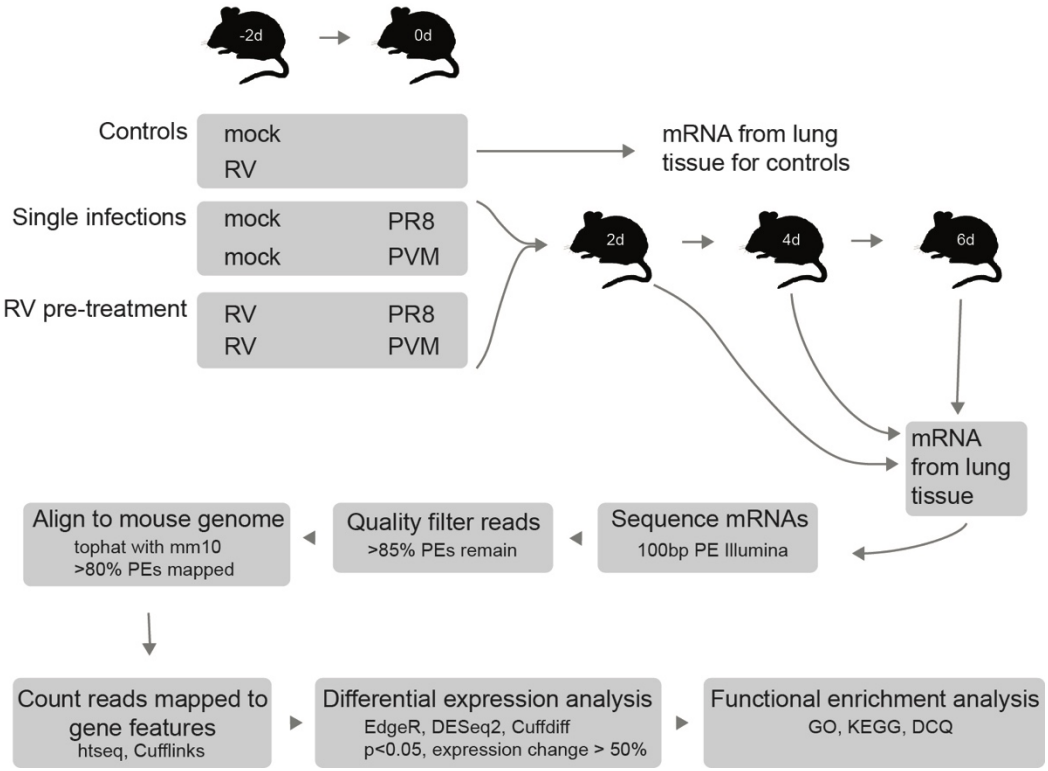

1083

1084

1085

1086

1087

1088

1089

1090

1091

1092

1093

1094

1095

1096 **Figure 3.**

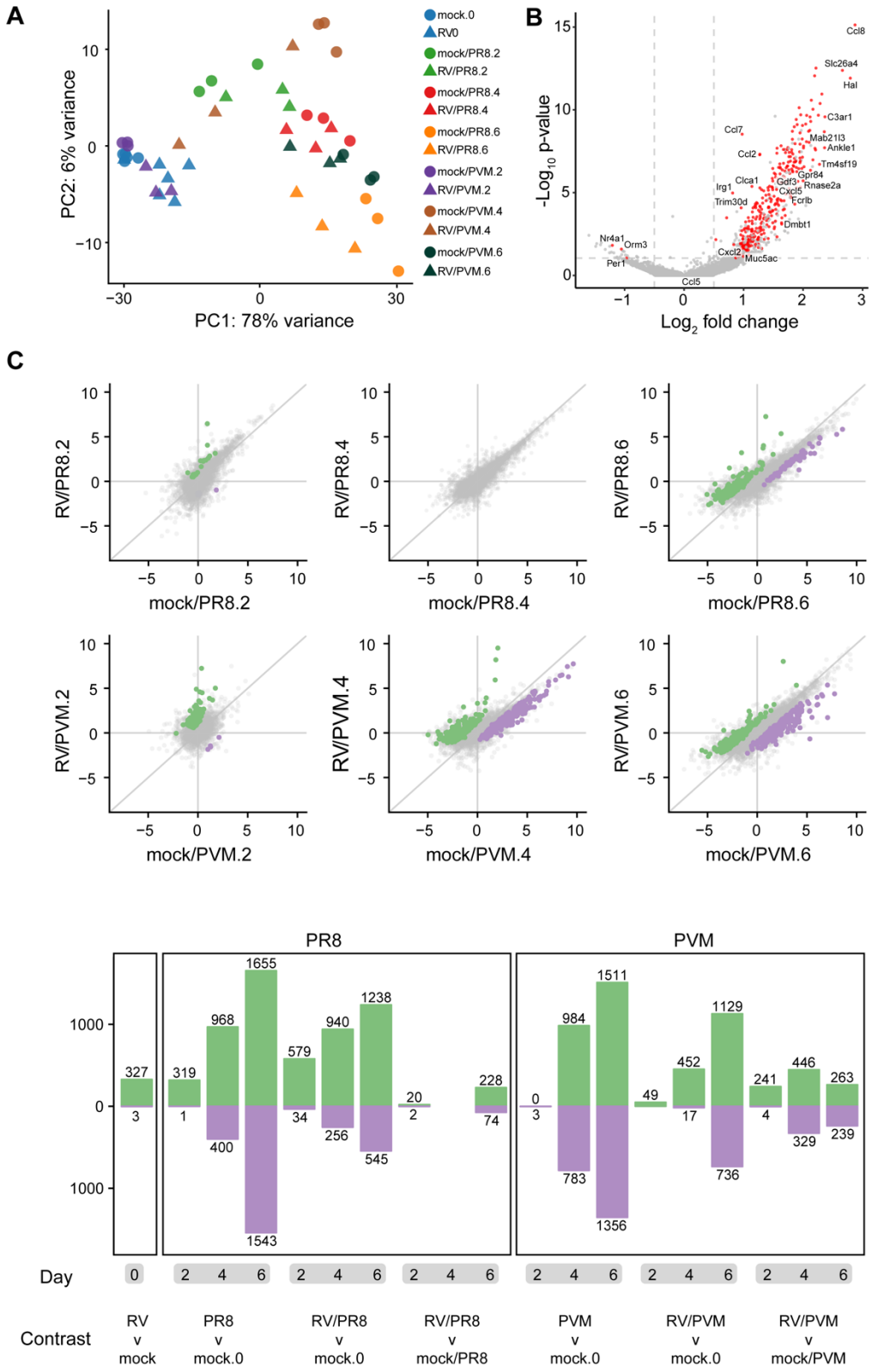

1097

1098 **Figure 4.**

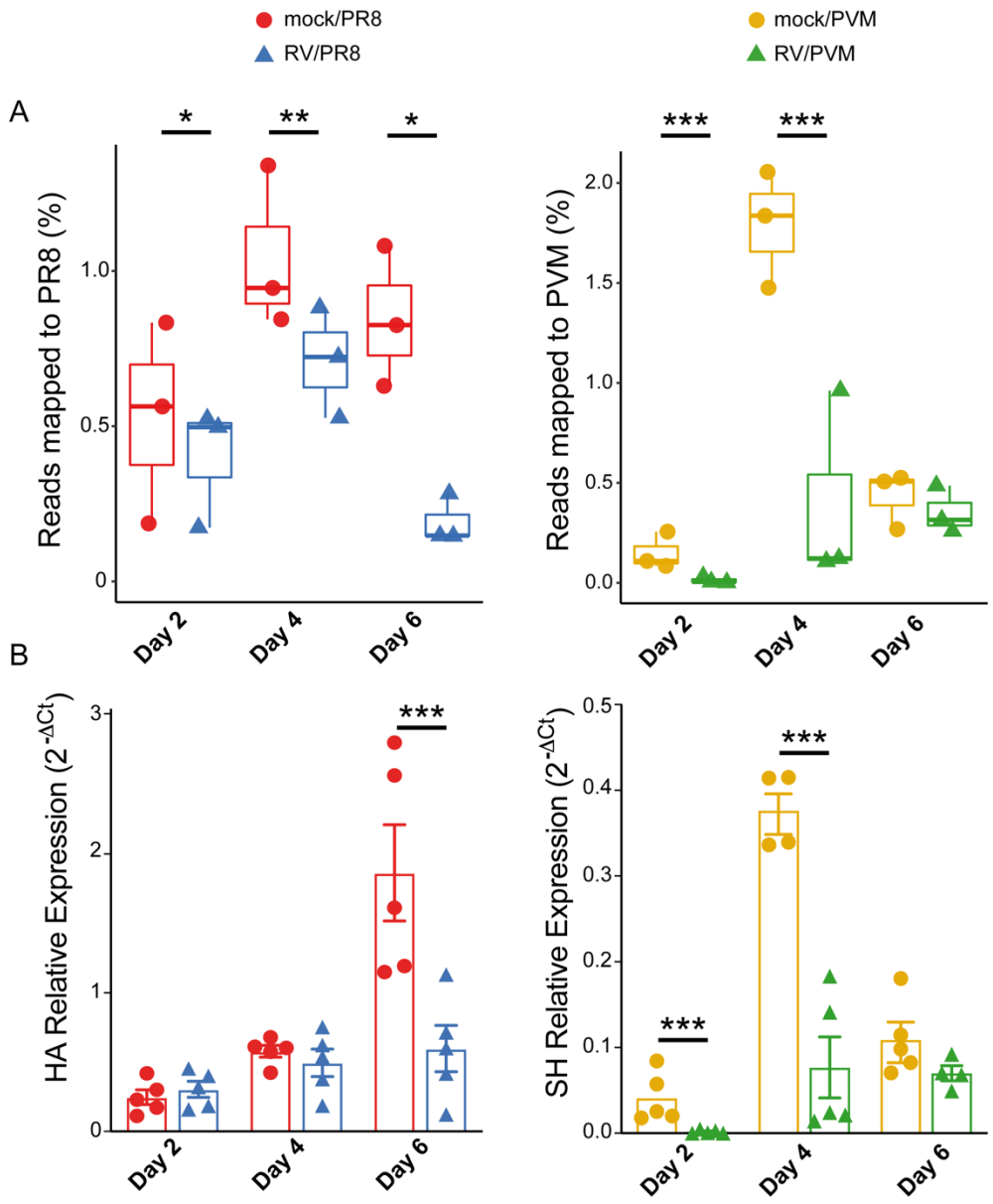

1099

1100

1101

1102

1103

1104

1105 **Figure 5.**

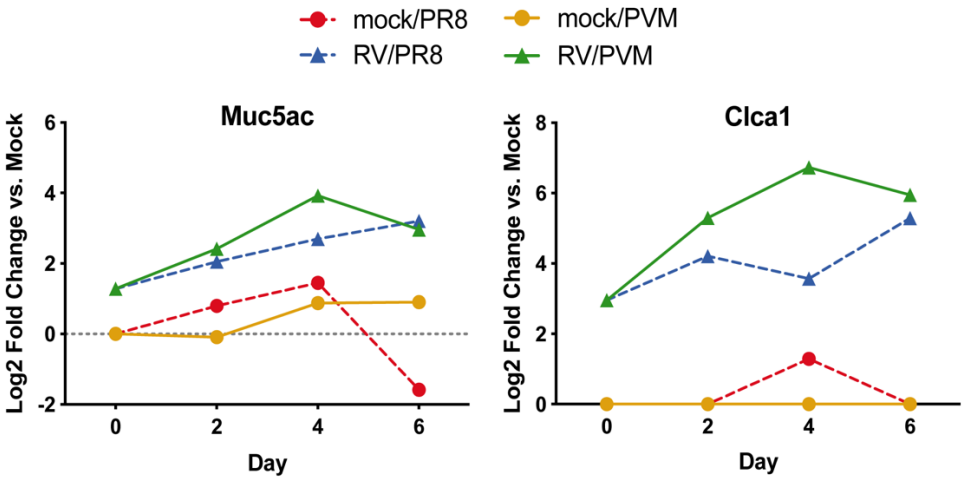

1106

1107

1108

1109

1110

1111

1112

1113

1114

1115

1116

1117

1118

1119

1120

1121

1122 **Figure 6.**

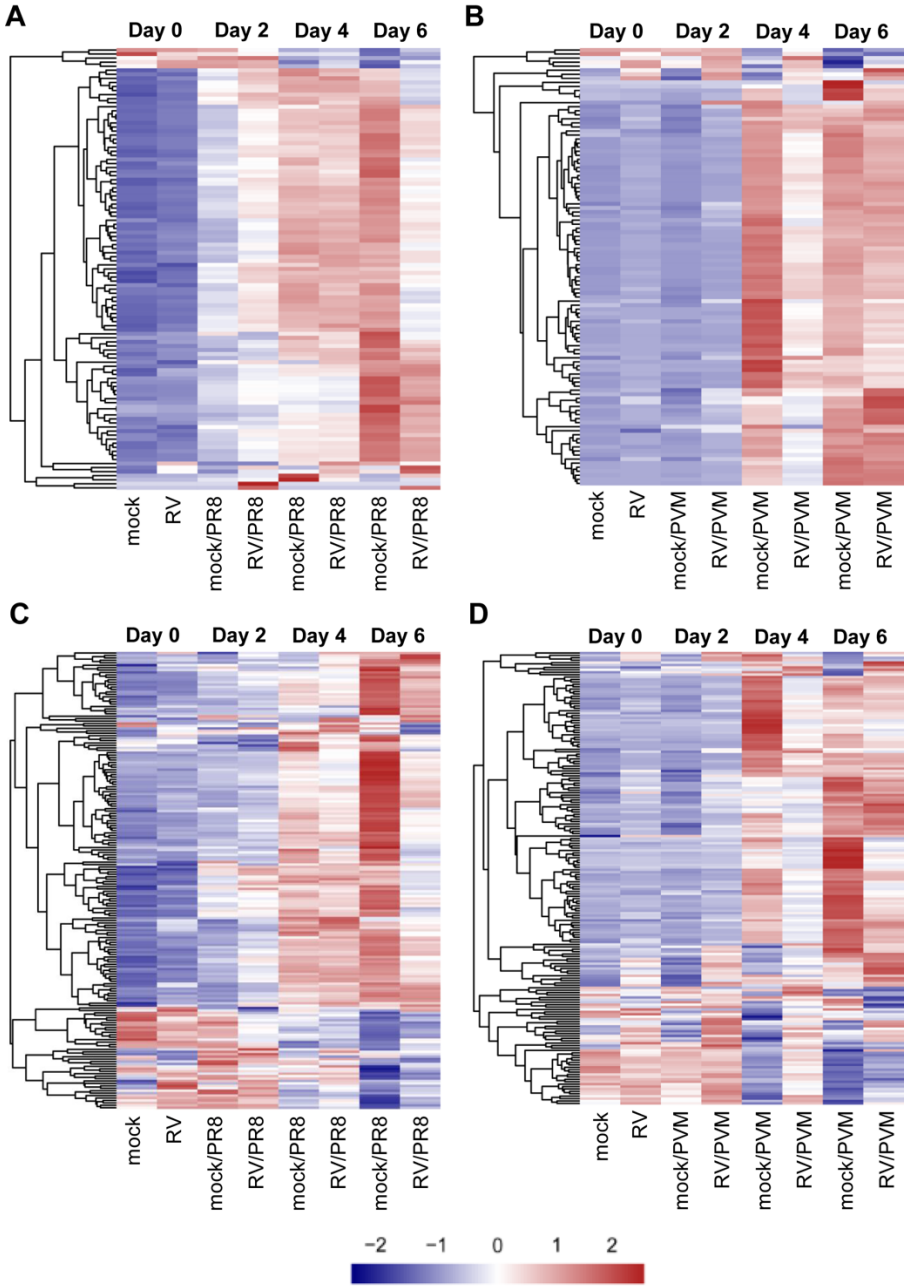

1123

1124

1125

1126

1127

1128 **Figure 7.**

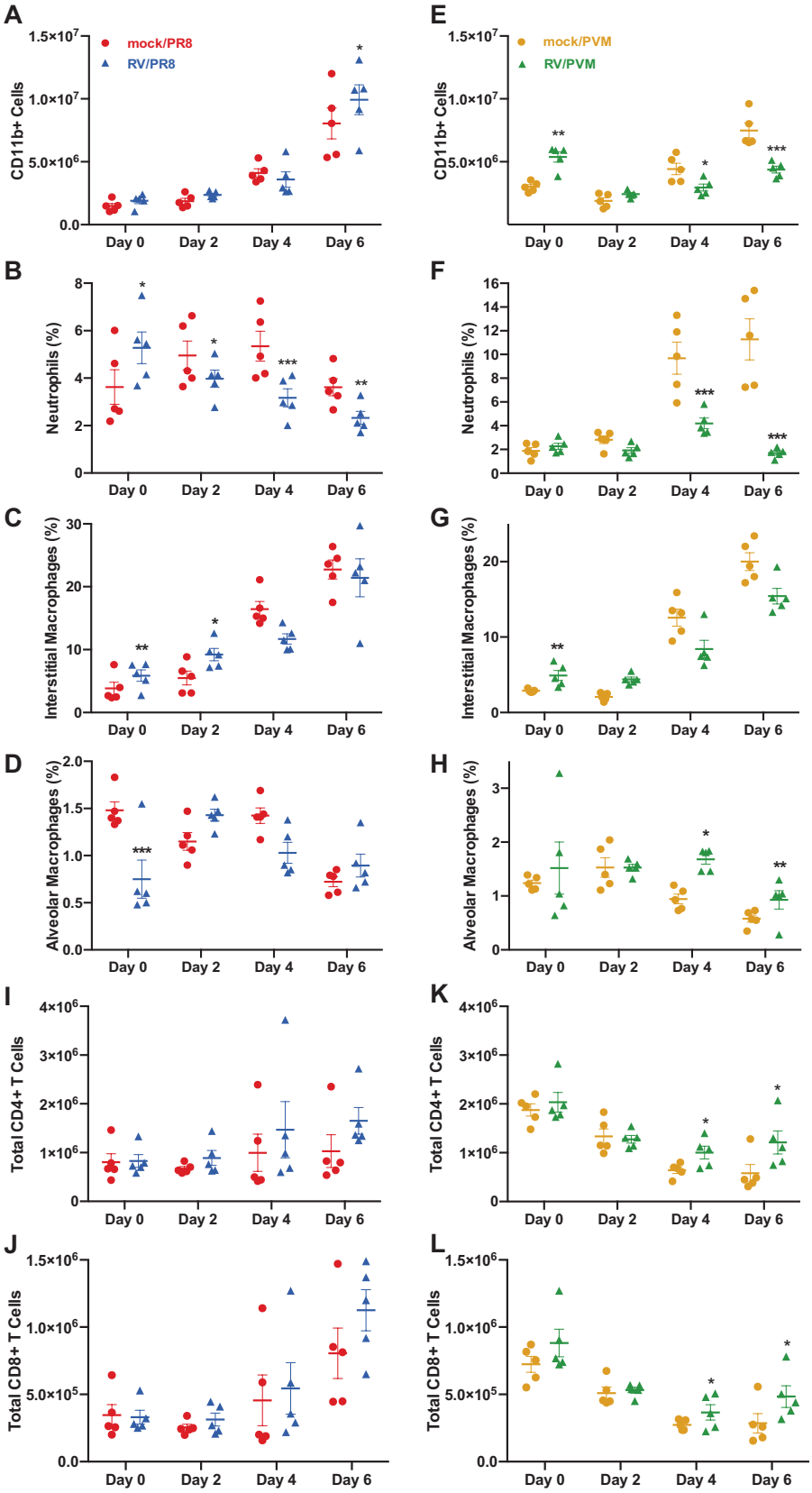

1129

1130 **Figure 8.**

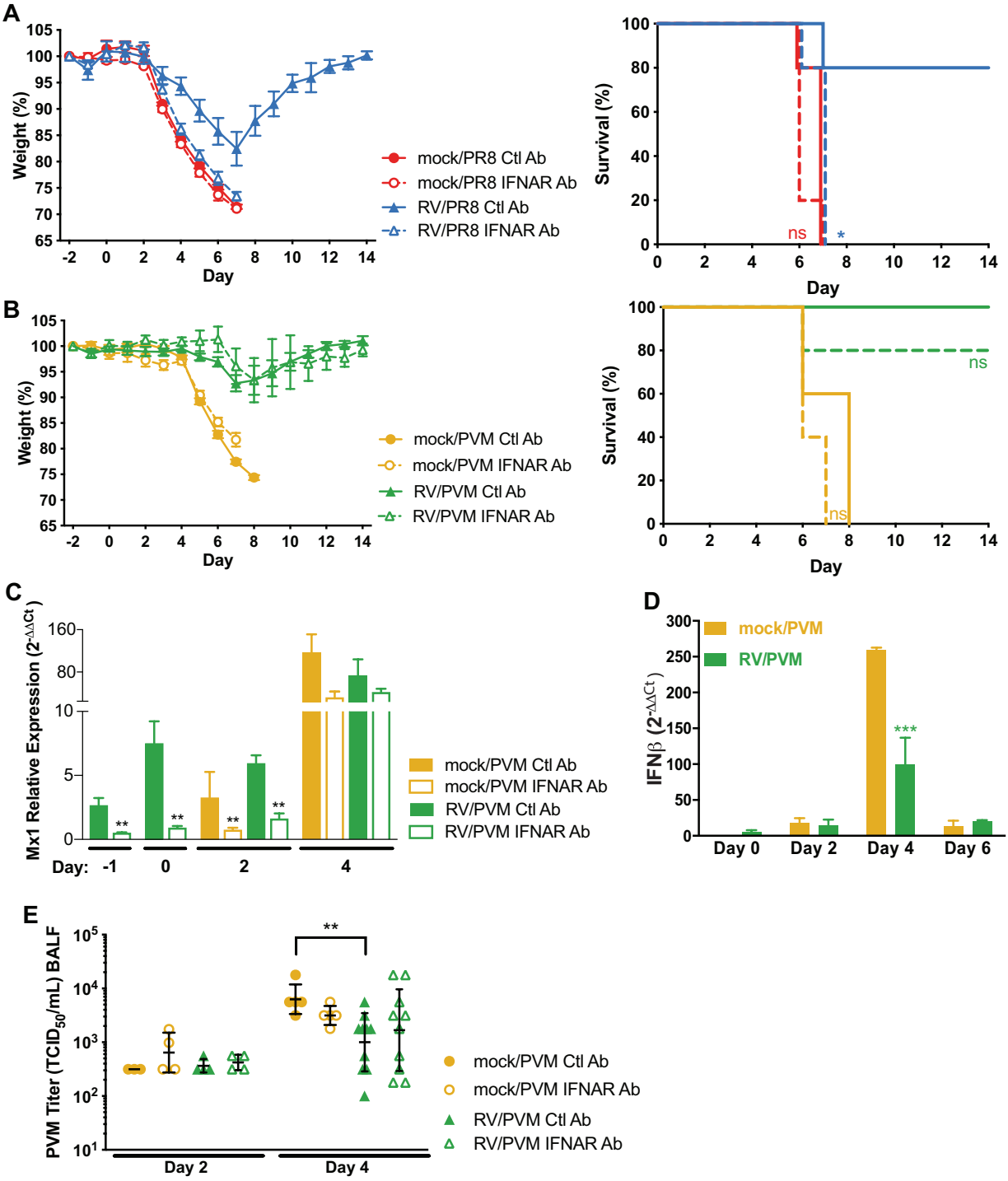

1131

1132

1133

1134

1135 **Figure 9.**

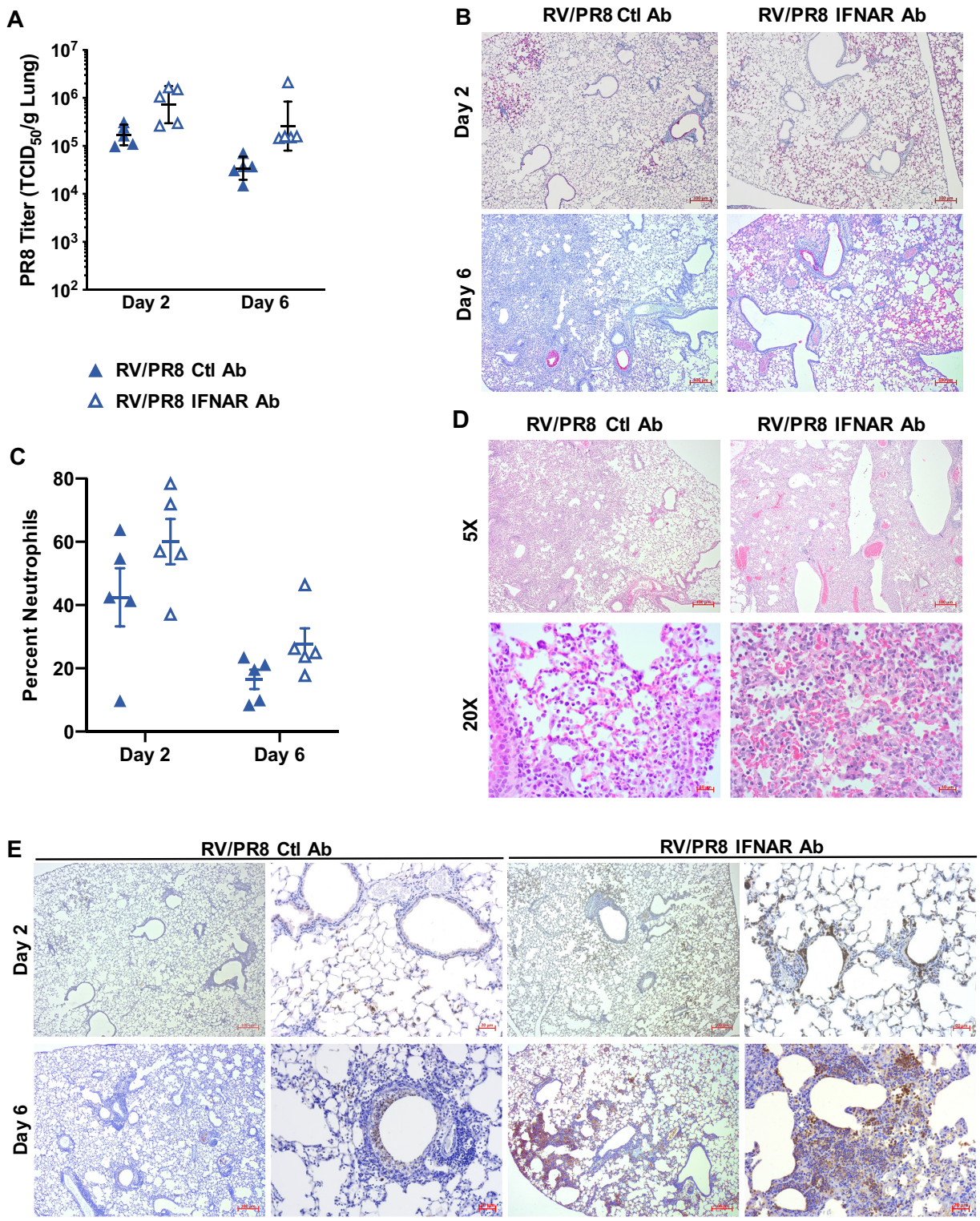

1136

1137

1138 **Figure 10**

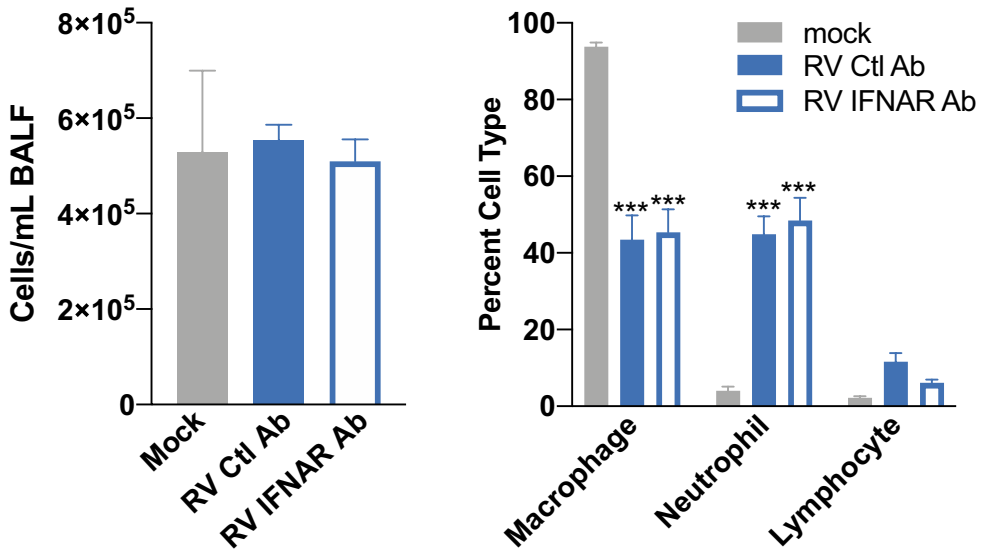

1139

1140